Human Molecular Genetics, 2007, Vol. 16, No. 23 ***2816–2833***
doi:10.1093/hmg/ddm238
Advance Access published on August 29, 2007

Nesprin-1 and -2 are involved in the pathogenesis of Emery–Dreifuss muscular dystrophy and are critical for nuclear envelope integrity

Qiuping Zhang[1], Cornelia Bethmann[3], Nathalie F. Worth[1], John D. Davies[1], Christina Wasner[3], Anja Feuer[3], Cassandra D. Ragnauth[1], Qijian Yi[1], Jason A. Mellad[1], Derek T. Warren[1], Matthew A. Wheeler[4], Juliet A. Ellis[4], Jeremy N. Skepper[2], Matthias Vorgerd[5], Beate Schlotter-Weigel[6], Peter L. Weissberg[1], Roland G. Roberts[7], Manfred Wehnert[3] and Catherine M. Shanahan[1]*

[1]Department of Medicine and [2]Multi-Imaging Centre, Physiology Development and Neuroscience, Anatomy Building, University of Cambridge, Cambridge, UK, [3]Institute of Human Genetics, University of Greifswald, Greifswald, Germany, [4]Randall Division of Cell and Molecular Biophysics, Kings College London, London, UK, [5]Neurologische Univ.-Klinik Bergmannsheil Ruhr-Universitat Bochum, Burkle-de-la-Camp-Platz 1, D-44789 Bochum, Germany, [6]Department of Neurology, Friedrich Baur Institute, University of Munich, Ziemssentr. 1a, D-80336 Munich, Germany and [7]Division of Medical and Molecular Genetics, Kings College London, 8th Floor, Guy's Tower, Guy's Hospital, London SE1 9RT, UK

Received July 5, 2007; Revised and Accepted August 21, 2007

Emery–Dreifuss muscular dystrophy (EDMD) is a heterogeneous late-onset disease involving skeletal muscle wasting and heart defects caused, in a minority of cases, by mutations in either of two genes encoding the inner nuclear membrane (INM) proteins, emerin and lamins A/C. Nesprin-1 and -2 are multi-isomeric, spectrin-repeat proteins that bind both emerin and lamins A/C and form a network in muscle linking the nucleoskeleton to the INM, the outer nuclear membrane, membraneous organelles, the sarcomere and the actin cytoskeleton. Thus, disruptions in nesprin/lamin/emerin interactions might play a role in the muscle-specific pathogenesis of EDMD. Screening for DNA variations in the genes encoding nesprin-1 (*SYNE1*) and nesprin-2 (*SYNE2*) in 190 probands with EDMD or EDMD-like phenotypes identified four heterozygous missense mutations. Fibroblasts from these patients exhibited nuclear morphology defects and specific patterns of emerin and SUN2 mislocalization. In addition, diminished nuclear envelope localization of nesprins and impaired nesprin/emerin/lamin binding interactions were common features of all EDMD patient fibroblasts. siRNA knockdown of nesprin-1 or -2 in normal fibroblasts reproduced the nuclear morphological changes and mislocalization of emerin and SUN2 observed in patient fibroblasts. Taken together, these data suggest that EDMD may be caused, in part, by uncoupling of the nucleoskeleton and cytoskeleton because of perturbed nesprin/emerin/lamin interactions.

INTRODUCTION

Emery–Dreifuss muscular dystrophy [EDMD; McKusick 310300 (1)] is a genetically heterogeneous neuromuscular disorder associated with early contractures, slowly progressive skeletal muscle wasting and weakness and cardiomyopathy, usually presenting as heart block in the second decade or later, with risk of sudden death (2). So far, two genes have

*To whom correspondence should be addressed at: Division of Cardiovascular Medicine, Addenbrooke's Centre for Clinical Investigation, Box 110, Addenbrooke's Hospital Hills Road, Cambridge CB2 2QQ, UK. Tel/Fax: +44 1223331504/5; Email: cs131@mole.bio.cam.ac.uk

been associated with EDMD. Mutations in the *EMD* (*STA*) gene-encoding emerin, an inner nuclear membrane (INM) protein of unknown function, cause the X-linked form of EDMD (3). Mutations in the *LMNA* gene-encoding lamins A and C, intermediate filament proteins of the scaffold underlying the INM that bind to emerin, cause an autosomal dominant form (AD-EDMD) (4). Onset, course and severity including heart involvement can vary remarkably and are not obviously correlated with the type of mutation (5).

Mutations in the *LMNA* gene also cause a number of other disease phenotypes, commonly known as laminopathies, that include autosomal-dominant limb girdle muscular dystrophy type 1B (LGMD1B), dilated cardiomyopathy with conduction defects, Charcot–Marie–Tooth neuropathy type 2B1 (CMT2B1), Dunnigan's familial partial lipodystrophy, mandibuloacral dysplasia (MAD1), premature ageing syndromes such as Hutchinson–Gilford progeria syndrome, atypical Werner's syndrome and restrictive dermopathy as well as a variety of other clinically overlapping disorders (6). For many of these disorders including EDMD, there is variable penetrance (7) and phenotypic heterogeneity (8), suggesting that mutations in other presently unknown modifier genes may contribute to the variable phenotypic expression of the diseases. Importantly, ~60% of patients with EDMD or EDMD-like phenotypes do not have mutations in either *EMD* or *LMNA* (9). Most of these remaining cases are sporadic further suggesting the involvement of other gene products and/or a role for a 'double-hit' or modifiers in expression of the disease phenotype (9). Likely, candidates are binding partners of emerin and lamin at the INM, particularly those highly expressed in muscle tissues.

Nesprins are a recently characterized family of spectrin-repeat proteins (10–14). Alternate initiation and splicing of two genes, *SYNE1* and *SYNE2*, generate multiple isoforms that vary greatly in size (15). Isoforms are variously composed of a spectrin-repeat rod domain linked to a C-terminal transmembrane KASH (Klarsicht-ANC-Syne-homology) domain, which mediates nuclear membrane localization, and/or N-terminal paired calponin-homology domains that bind actin. Nesprin isoforms are present in multiple sub-cellular locations including the nucleus, INM and outer nuclear membrane (ONM), in association with organelles such as mitochondria, Golgi apparatus and sarcoplasmic reticulum, throughout the muscle sarcomere including the Z-line, A/I junction, M-line and at the plasma membrane and thus form a network linking these structures to the actin cytoskeleton (15). Specific INM isoforms are highly expressed in the muscle and the heart and bind lamin A and emerin *in vitro* and *in vivo*. Like emerin, the retention of specific nesprin isoforms at the INM is dependent on lamin A binding (11,16–20), whereas the retention of emerin at the INM is also dependent on nesprin binding. Importantly, by binding to lamins and emerin, nesprins link the nucleoskeleton and INM to the ONM and cytoskeleton by forming a bridging LINC complex with the SUN-domain containing proteins, SUN1 and SUN2 across the luminal space between the INM and ONM (21). Therefore, we hypothesized that disruption of nesprin/lamin/emerin interactions may play a role in the complex tissue specific and currently unexplained aetiology of EDMD.

RESULTS

SYNE1 and SYNE2 sequence variants occur in EDMD patients without lamin and emerin mutations

Mutation screening of the *SYNE1* and *SYNE2* genes was performed in 190 EDMD and EDMD-like patients lacking *LMNA* or *EMD* mutations. Sixty-six exons for nesprin-1 corresponding to isoforms nesprin-1α_1, -1α_2, 1$\alpha\Delta$3SR, 1β_1 and 1β_2, 1$\beta\Delta$13SR as well as 22 exons for nesprin-2 corresponding to isoforms 2α_1, 2α_2, 2β_1 and 2β_2 were screened. This selection was based on high and specific expression of these isoforms in skeletal muscle and heart tissue as well as mapping of the emerin and lamin A/C-binding sites to domains within these isoforms (Fig. 1 and Supplementary Material, Fig. S1). Twenty-nine single nucleotide polymorphisms (SNPs) with frequencies between 1.0 and 48.4% and nine rare variants with frequences between 0.6 and 1% in a reference population ($n = 384$ alleles) were identified. The SNPs/variants included intronic sequence variations ($n = 10$), variations in the 3′- and 5′-untranslated region (UTRs) ($n = 11$), synonymous amino acid exchanges ($n = 6$) and non-synonymous amino acid exchanges ($n = 11$). All SNPs and variants have been submitted to an SNP database (http://www.ncbi.nlm.nih.gov/projects/SNP). In addition to these SNPs/variants, six unique DNA variants not present in 384 control alleles of an ethnically matched reference population were identified (Table 1). Two of these unique variants were in 5′-UTRs and four resulted in amino acid exchange: R257H, V572L and E646K in nesprin-1α and T89M in nesprin-2β. The amino acids changed by these missense mutations were in regions that were evolutionarily well conserved and within the mapped emerin and lamin binding domains in nesprin-1 and nesprin-2 (Fig. 1A and B).

Segregation was analysed in the families of affected individuals (Fig. 2). All index cases but one (G-11774, family 2), who was a double heterozygote for nesprin-1α V572L and nesprin-2β T89M, were heterozygous for one mutation: nesprin-1α R257H (G-12552, family 1), nesprin-1α E646K (G-12214, family 3) and nesprin-2β T89M (G-9539, family 4), respectively. The disease occurred sporadically in family 1, with the nesprin-1α R257H mutation possibly present in the early deceased father, as well as family 3 with the nesprin-1α E646K mutation (the family being unavailable for screening). In families 2 and 4 with the *SYNE2* T89M mutation, the segregation pattern was compatible with autosomal-dominant inheritance as the mutation co-segregated with the disease. The clinical expression of the disease phenotype was variable, ranging from almost asymptomatic moderately increased creatinine kinase level in family 3 to muscular dystrophy combined with severe dilated cardiomyopathy requiring heart transplantation at age 26 in the double heterozygous proband G-11774 of family 2 (see Supplementary Material). All available patients (Supplementary Material, Table S1) with a putative pathogenic mutation in the *SYNE1* or *SYNE2* genes were included in further cell biological investigations.

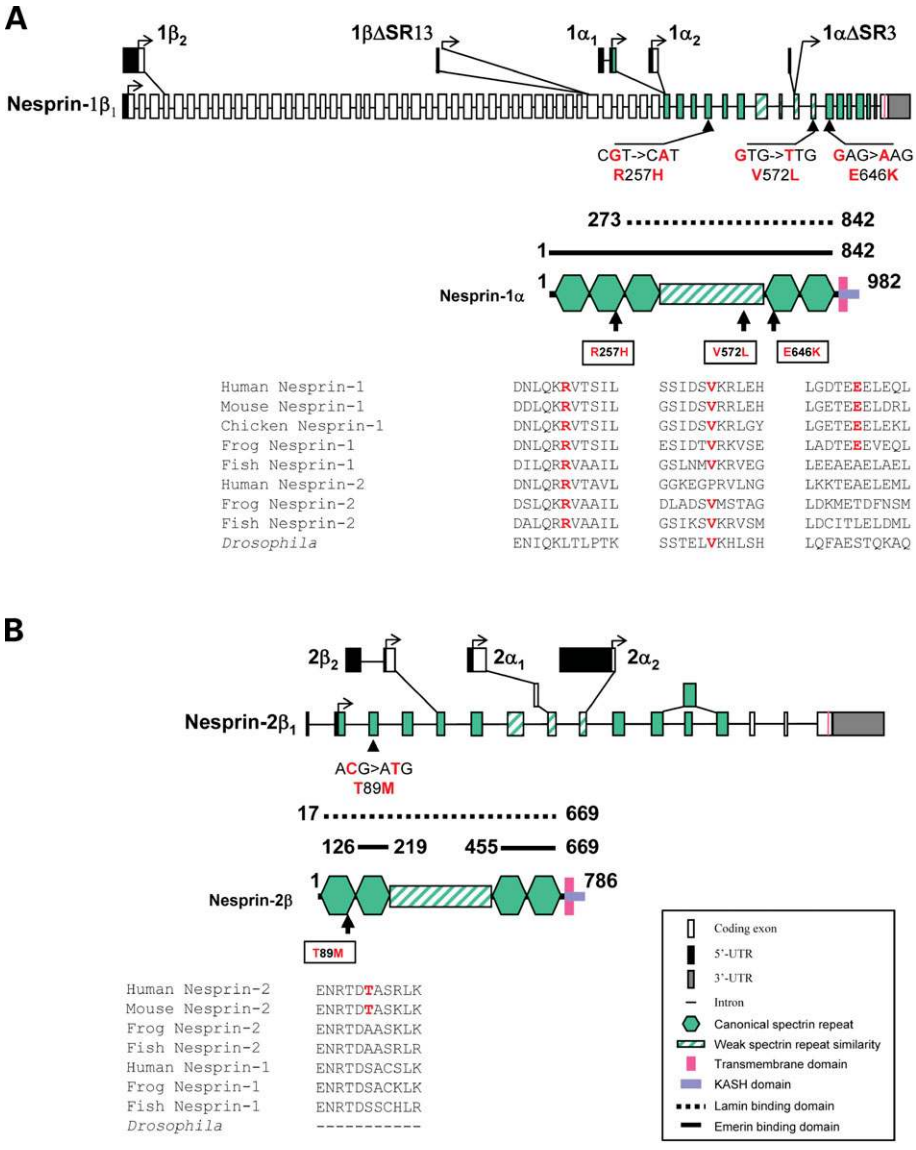

Figure 1. *Identification of nesprin-1 and -2 sequence variants in EDMD patients*. Map of the exons screened for DNA sequence variants showing alternate initiation sites for different isoforms in nesprin-1 (**A**) and nesprin-2 (**B**). Evolutionary conservation of the amino acid changes caused by missense mutations is shown in the context of INM isoforms. Mapped emerin (bold line) and lamin (dashed line) binding domains within these nesprin-1 and -2 isoforms are shown.

Table 1. Rare (≤1%) nesprin-1 and -2 sequence variants identified in EDMD patients

Gene and exon	DNA variation	Amino acid exchange	Allele frequency in patients	Allele frequency in a reference population (%)	Patients
1α, 6	c.966G > A	p.R257H	0.37, $n = 268$	0.00, $n = 384$	Family 1: II(1)
1α, 12	c.1910G > T	p.V572L	0.37, $n = 268$	0.00, $n = 384$	Family 2: I(1), II(1)
1α, 13	c.2132G > A	p.E646K	0.37, $n = 268$	0.00, $n = 384$	Family 3: II(1)
$1\beta_1$, 3	c.466C > T	p.T89M	0.53, $n = 380$	0.00, $n = 384$	Family 2: I(2), II(1); family 4: I(1), II(1), II(2).
1α2, N-terminus	29A > G	5′-UTR	0.26, $n = 380$	0.00, $n = 384$	—
2α2, 1	525G > A	5′-UTR	0.53, $n = 380$	0.00, $n = 384$	—

References sequences: nesprin-$1\alpha_1$: AY061756, $1\alpha_2$: AY184203, nesprin-$1\beta_1$: AY061755, $1\beta_2$: AY184206, nesprin-$2\alpha_1$: AY061758, nesprin-$2\alpha_2$: AY184204, nesprin-2β: AY061757. *n*, number of alleles analysed.

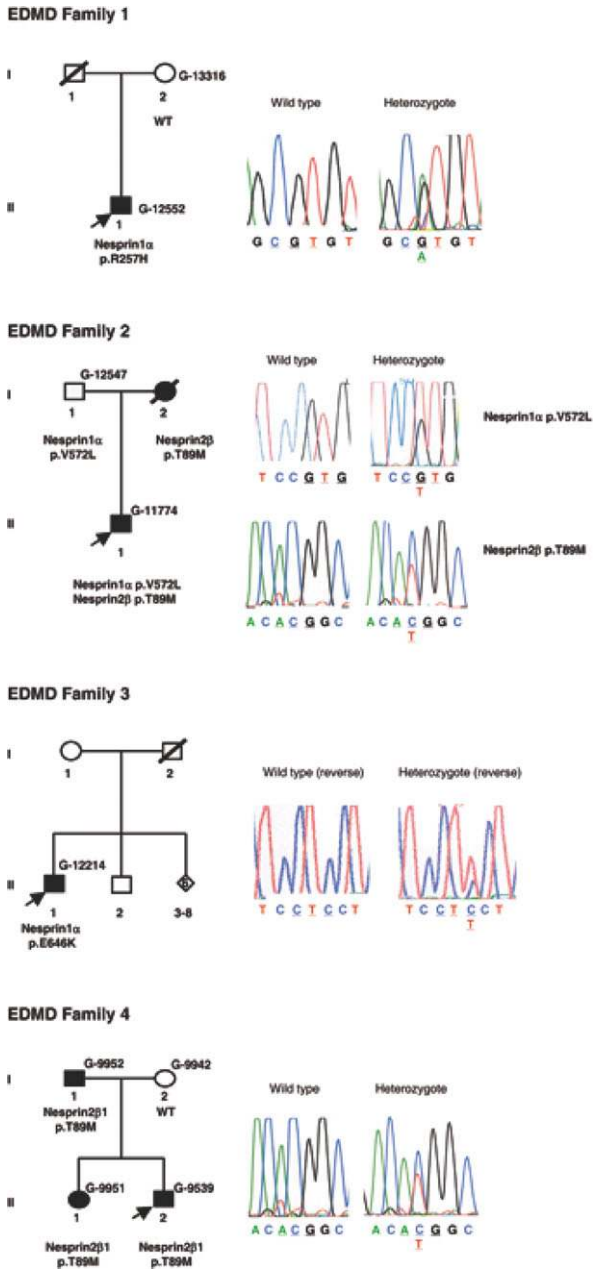

Figure 2. Pedigrees of probands showing segregation of *SYNE1* and *SYNE2* sequence variants and sequencing data.

Fibroblasts from EDMD patients with SYNE1 and SYNE2 mutations show nuclear defects and mislocalization of nesprin, emerin and lamin

Skin fibroblasts from EDMD patients with *SYNE* mutations showed similar defects in nuclear morphology to those described in patients with *EMD* and *LMNA* mutations (22,23). DAPI staining of interphase nuclei demonstrated that, in contrast to the normal ovoid morphology seen in the majority of control fibroblasts, *SYNE1* and *SYNE2* mutant fibroblasts exhibited a convoluted appearance as well as micronuclei, giant and fragmented nuclei (Fig. 3A and B). Heterogeneous DAPI labelling of nuclear lobules suggested that the nuclear shape abnormalities were accompanied by chromatin reorganization. In ~8% of patient cells (compared with <0.5% in controls), staining with antibodies to lamin A/C and lamin B1 showed the typical 'honeycomb' pattern, indicative of loss of NE integrity in EDMD fibroblasts. In these cells, intranuclear lamin A/C also stained weakly and was often mislocalized into punctate dots (Fig. 3C). Nuclear defects were scored for patients and controls at multiple passage numbers (p11–14) and were significantly different at all stages, suggesting that they were not due to culture artefacts.

Using nesprin antibodies recognizing epitopes within the isoforms screened, western blot showed that the levels of nesprin-1 and -2 were not different between patients and controls (data not shown). However, using immunofluorescence, the subcellular localization of nesprin-1 and -2 was altered in fibroblasts from EDMD patients. In control cells, nesprin-1 was clearly present in the nucleus, at the NE, and in mitochondria. However, the NE and mitochondrial localizations were reduced or lost in patient fibroblasts. Similarly, nesprin-2 was present at the NE in control cells and this staining was reduced in EDMD fibroblasts (Fig. 4A). Importantly, this reduction in nesprin-1 and nesprin-2 NE staining, which was apparent in ~50% of cells, was also observed in fibroblasts from patients with *LMNA* ($n = 3$) and *EMD* ($n = 3$) (Fig. 4A) mutations, suggesting that loss of NE nesprins is characteristic of EDMD.

A feature unique to fibroblasts derived from EDMD patients with *SYNE* mutations was the mislocalization of emerin. In a significant proportion of interphase nuclei, emerin was virtually lost from the NE and instead incorporated into micronuclei associated with the nucleus or was concentrated in a polar cap at one end of a honeycomb nucleus (Fig. 4B–D). In these cells, nesprin–emerin co-localization at the NE was lost and nesprin was not co-localized with emerin in the micronuclei or the polar caps (Fig. 4B). SUN2 was also mislocalized in these cells and co-localized with emerin in the polar caps (Fig. 4C), whereas SUN1 was unaffected (data not shown). Emerin was mislocalized to the cytoplasm in a significant proportion of fibroblasts with the *SYNE2* T89M mutation (Fig. 4D and E) and other defects observed included concentrations of emerin in intranuclear tubules and persistent emerin 'bridges' connecting telophase cells (data not shown) suggestive of a failure of NE reformation after cell division (24) (Fig. 4B–E).

Nesprins are absent from the NE in skeletal muscle from EDMD patients

Emerin and lamin mislocalization defects similar to those observed in fibroblasts were also observed in myoblasts ($n = 2$) from patients with *SYNE* mutations. (Supplementary Material, Fig. S2). Myoblasts from these patients showed impaired *in vitro* differentiation when compared with those from controls or patients with *LMNA* mutations (Fig. 5A and B). Moreover, the sarcomeric structures that formed *in vitro* were less well defined than in controls with nesprin-1 and -2 not correctly localized to sarcomeric bands but diffusely distributed (Fig. 5A).

Changes in nesprin and emerin NE localizations were also apparent in muscle tissue sections from EDMD patients (Fig. 5C). In control muscle, nesprin-1 and -2 antibodies

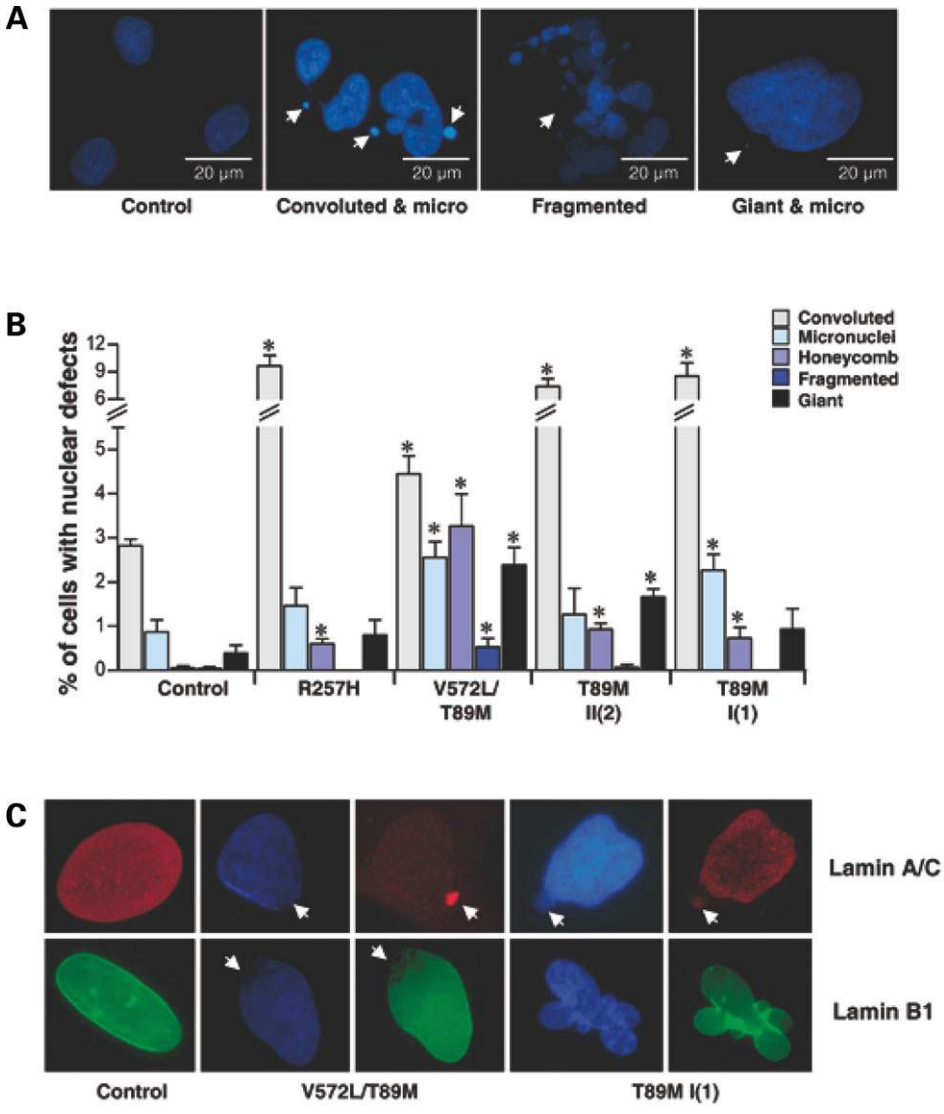

Figure 3. Nuclear defects and lamin mislocalization in EDMD patient fibroblasts. (**A**) DAPI-stained nuclei from EDMD patients with *SYNE* mutations showing nuclear morphology defects; control (panel 1), convoluted and micronuclei (arrowed, panel 2), fragmented nuclei (panel 3) and giant convoluted nuclei with micronucleus (arrowed) (panel 4). (**B**) Graphical representation of the frequency of nuclear defects in each patient. $N = 500$ nuclei were counted in more than three individual experiments and results are presented as mean ± SEM and analysed by independent samples *t*-test with $^{*}P < 0.05$. Each significant *P*-value (mutant versus control) is as follows: for convoluted nuclei: R257H, $P = 0.001$; V572L/T89M, $P = 0.021$; T89M II(2), $P = 0.002$; T89M I(1), $P = 0.005$; for micronuclei: V572L/T89M, $P = 0.012$; T89M I(1), $P = 0.024$; for honeycomb: R257H, $P = 0.005$; V572L/T89M, $P = 0.003$; T89M II(2), $P = 0.001$; T89M I(1), $P = 0.022$; for fragmented nuclei: V572L/T89M, $P = 0.007$; for giant nuclei: V572L/T89M, $P = 0.007$; T89M II(2), $P = 0.004$. (**C**) Honeycombing of the nucleus and defects in lamin A/C (arrowed) and B1 localization in EDMD fibroblasts with *SYNE* mutations. Note mislocalization and loss of intranuclear lamin A/C staining (top panels). Lamin B1 staining is absent from regions of honeycombed nucleus (arrowed) (bottom panels).

labelled the NE and co-localized with emerin. In contrast, in the compound heterozygote patient G-11774 (*SYNE* V572L/T89M) emerin staining was reduced, mislocalized or lost from sarcomeric nuclei and only present in fibroblast nuclei, which lacked nesprin-2 staining. NE nesprin-1 was also lost from sarcomeric nuclei and the sarcomeric staining observed with this antibody was disrupted (Fig. 5C). In a patient with XL-EDMD (del exon 6 of *EMD*, G-12704), loss of nesprin-1 and -2 from the NE was also observed in 50% of nuclei (Supplementary Material, Fig. S2), further suggesting that loss of NE nesprin is a characteristic feature of EDMD.

Nesprin/emerin/lamin binding interactions are disrupted in EDMD patient fibroblasts

The mislocalization of emerin in fibroblasts and myoblasts from EDMD patients with *SYNE* mutations led us to investigate the binding relationship between nesprin and emerin at the NE. Overexpression of green fluorescent protein (GFP)-tagged nesprin-1 and -2 isoforms (nesprin-1α, nesprin-1βΔ13SR, nesprin-2α and 2β) that target to the NE all caused mislocalization of emerin from the INM in U2OS cells and human dermal fibroblasts (HDFs), with the effects of nesprin-1 more dramatic than nesprin-2 (Fig. 6). Mislocalization of emerin also occurred

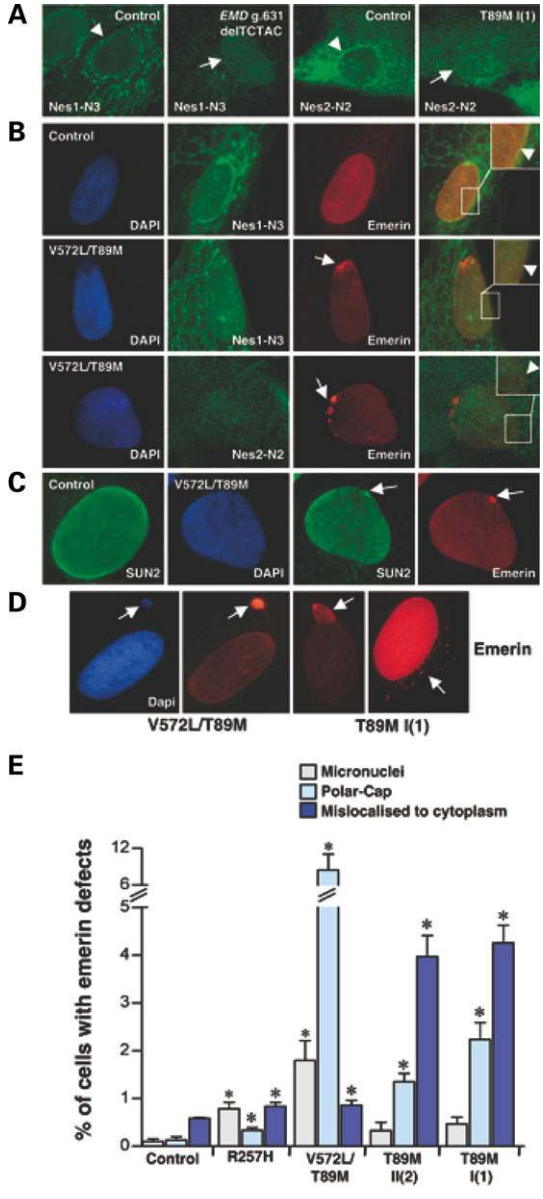

Figure 4. Nesprin, emerin and SUN2 mislocalization in EDMD patient fibroblasts. (**A**) NE nesprin-1 and -2 staining was lost or diminished in EDMD fibroblasts mutations (arrowed), compared with controls (arrowhead). Fibroblasts from patients with *EMD* and *SYNE2* mutations shown. (**B**) In control fibroblasts, emerin and nesprin co-localize at the NE (arrowhead) (top panels). Co-localization was not observed in a proportion of fibroblasts from patients with *SYNE* mutations where emerin was mislocalized to a polar cap (arrowed). Boxed regions show enlargement. (**C**) In cells where emerin was mislocalized, SUN2 was also mislocalized to the polar cap (arrowed). (**D**) Emerin defects observed in *SYNE* mutant patient fibroblasts included localization of emerin to a micronucleus (panels 1 and 2), honeycombing and polar cap localization of emerin (panel 3) and mislocalization of emerin to the cytoplasm (panel 4). (**E**) Graphical representation of the frequency of emerin defects observed in EDMD patient fibroblasts with *SYNE* mutations. $N = 500$ cells were counted in more than three independent experiments at different passage numbers. The results are presented as mean $\pm$ SEM. $^{*}P < 0.05$ was defined as statistical significance analysed by independent samples *t*-test. Each significant *P*-value (mutant versus control) is as follows: for micronuclei: R257H, $P = 0.010$; V572L/T89M, $P = 0.021$; for polar cap: R257H, $P = 0.050$; V572L/T89M, $P = 0.032$; T89M II(2), $P = 0.003$; T89M I(1), $P = 0.004$; for mislocalized to cytoplasm: R257H, $P = 0.039$; V572L/T89M, $P = 0.043$; T89M II(2), $P = 0.002$; T89M I(1), $P = 0.001$.

if nesprin-1α and -2βconstructs carrying the missense mutations were expressed (data not shown). Overexpression of nesprin isoforms had no effect on lamin A/C localization (data not shown).

Co-immunoprecipitation was used to investigate nesprin binding to emerin and lamin A/C in fibroblasts from EDMD patients. Using nesprin-1 and -2 antibodies, generally less emerin was co-immunoprecipitated from patient extracts harbouring *SYNE* or *LMNA* mutations when compared with controls. The amount of lamin A/C co-immunoprecipitated by nesprin-1 and nesprin-2 antibodies was consistently and significantly reduced in all EDMD patient extracts, compared with controls. In contrast, in fibroblasts extracts from patients with *LMNA* mutations causing progeria syndromes, co-immunoprecipitation of lamin A/C by nesprins was only slightly reduced (G608G *LMNA* mutation) or unaffected (S143F *LMNA* mutation) (Fig. 7A). These observations suggested that mutations in *SYNE*, *EMD* or *LMNA* that are causal in EDMD result in changes to the binding equilibrium of the nesprin/emerin/lamin protein complex at the INM.

A quantitative microtitre plate assay was used to investigate binding further. Nesprin-2β was found to bind more strongly to emerin than nesprin-1α; however, no change in binding was observed for the nesprin-2 T89M mutant. In contrast, nesprin-1α recombinant protein harbouring the nesprin-1 V572L amino acid change was found to bind more strongly to emerin than wild-type nesprin-1α (Fig. 7B), with binding of the nesprin-1 E646K variant unchanged from wild-type. The nesprin-1 V572L amino acid change occurs within the minimal nesprin-1/emerin binding domain (residues 373–627) and increased binding compared with wild-type was confirmed by the gel-overlay assay using only this region of nesprin-1 (Fig. 7C) (25). Binding of nesprin-1α and -2β to the C-terminal Ig-domain of lamin was also investigated in these assays; however, no differences in binding between wild-type and mutant forms of nesprin were observed (data not shown) (20).

SiRNA knockdown of nesprin-1 and nesprin-2 reiterates EDMD fibroblast nuclear defects and causes emerin mislocalization

The studies mentioned earlier suggested that stable nesprin interactions at the INM are important to maintain nuclear architecture. To investigate the effects of altering these binding relationships, multiple siRNAs were designed to regions of nesprin 1α($n = 3$) and 1β($n = 2$), and nesprin-2α ($n = 2$) transcripts and their effects on nuclear phenotype in fibroblasts and U2OS cells analysed.

Immunofluorescence demonstrated that siRNAs were able to diminish nesprin-1 and nesprin-2 proteins at the NE; however, nesprin staining in the cytoplasm was generally unaffected (Fig. 8A). Western blot confirmed knockdown of a number of bands corresponding in size to known nesprin-1 and nesprin-2 NE isoforms (Fig. 8B). Nesprin-1α siRNA reduced nesprin-1α (110 kDa) as well as smaller nesprin-1αΔ truncated isoforms, whereas nesprin-2 siRNA reduced nesprin-2α and -2β(~60 and 80 kDa, respectively). Nesprin-1β siRNA caused the greatest knockdown with complete loss of the smaller bands as well as larger bands

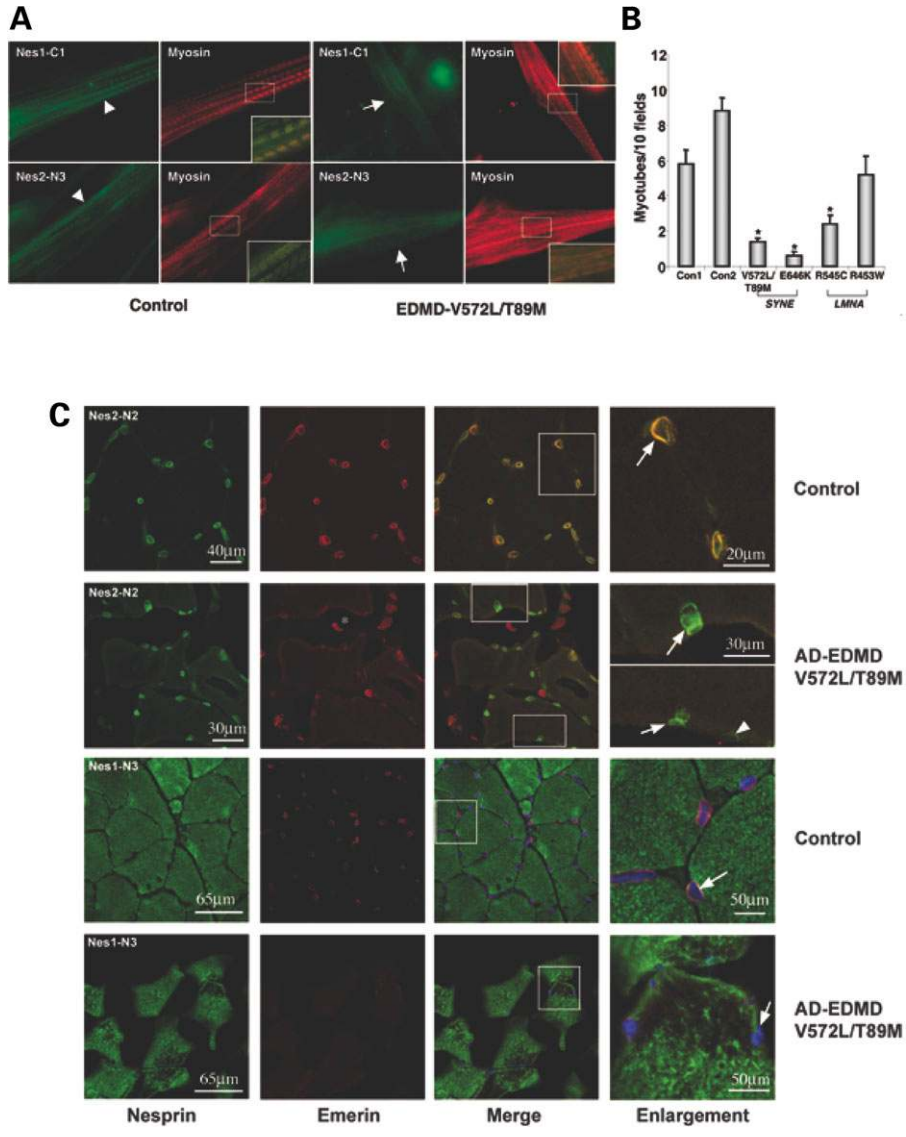

Figure 5. Nesprin defects in skeletal muscle from EDMD patients. (**A**) *In vitro* differentiation of myoblasts to myotubes was impaired in cells from patients with *SYNE* mutations. In contrast to control myotubes which formed well-defined sarcomeric structures with nesprin-1 and -2 localized to Z-bands and M-bands, respectively (arrowhead), myotubes from patients with *SYNE* mutations did not form well-organized sarcomeres and nesprin-1 and -2 staining was weak with no staining of sarcomeric structures and weak nuclear staining (arrowed). (**B**) Graphical representation of level of myotube differentiation defined by staining with myosin. $^{*}P < 0.05$ was defined as statistical significance analysed by independent samples *t*-test. $N = 10$ random fields counted in five independent experiments. Each significant *P*-value (mutant versus control no. 1) is as follows: *SYNE1* V572L/*SYNE2* T89M, $P = 0.001$; *SYNE1* E646K, $P < 0.0001$; *LMNA* R545C, $P = 0.007$. (**C**) The top panels show complete co-localization of nesprin-2 and emerin at the NE in control skeletal muscle tissue (arrowed). In the double heterozygote, *SYNE1* V572L/*SYNE2* T89M emerin was lost from the NE (arrowhead and arrows) and some nesprin-2 was mislocalized to the cytoplasm (arrowed) (second panels). Emerin staining was obvious only in fibroblasts (indicated by asterisk), which did not stain for nesprin-2. Similarly, in control tissue, nesprin-1 and emerin co-localized at the NE (arrowed) with nesprin-1 also distributed in the sarcomere at Z-lines (third panel). In the patient, both emerin and nesprin-1 were lost from the NE (arrowed) in the majority of nuclei (bottom panels) and sarcomeric staining was disrupted.

>160 kDa corresponding to isoforms related to nesprin-1β and nesprin-1βΔ truncated isoforms that are likely to be present on the ONM. qRT–PCR confirmed that siRNAs diminished levels of RNA transcripts encoding the KASH domains of both nesprin-1 and nesprin-2 (Fig. 8B).

siRNA treatment resulted in gross defects of nuclear morphology. These defects mimicked all those observed in EDMD patient fibroblasts and included convoluted nuclei, micronuclei, giant and fragmented nuclei (Fig. 8C and D) as well as 'honeycombing' of the nucleus associated with disrupted lamin A/C and B localization (Fig. 8E). Many of the larger nuclei appeared transparent on DAPI staining, suggesting that the 'nucleoskeleton' had been disrupted and the nucleus expanded. Indeed, both nesprin-1 and nesprin-2 siRNAs caused a significant increase in nuclear size (1.5- and 1.3-fold increase, respectively) in U2OS cells (Fig. 8C). However, each siRNA had subtly different effects on nuclear morphology. The major effect of the nesprin-1α siRNAs in both fibroblasts and U2OS cells was to cause convoluted nuclei, whereas the nesprin-1β siRNAs caused more

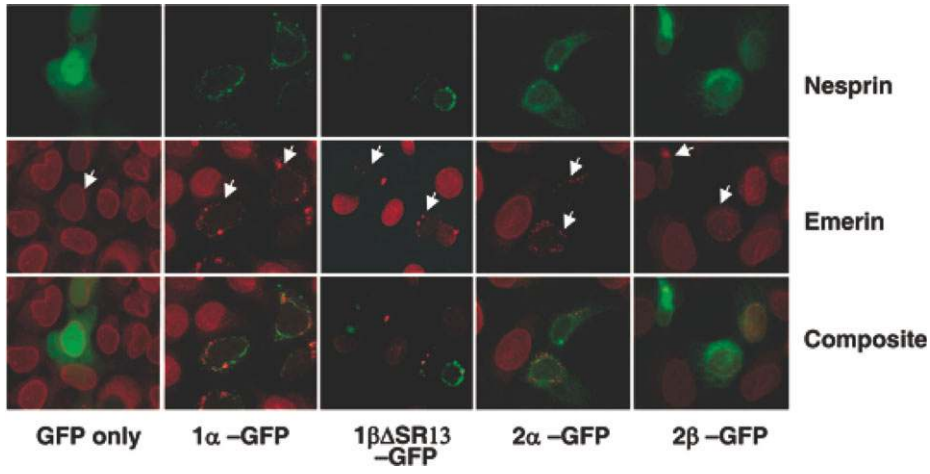

Figure 6. Emerin is mislocalized by exogenous expression of nesprin-1 and -2 isoforms. Overexpression of different nesprin-1 and -2 EGFP-tagged isoforms mislocalize emerin from the INM (arrowed) in U2OS cells.

honeycombing of the nucleus in fibroblasts. Nesprin-2 siRNAs generally had a less dramatic effect on nuclear morphology, but also caused a significant increase in honeycombing, particularly in U2OS cells. Western blot showed that this honeycombing of the nucleus was associated with reduced levels of lamin A/C and B as well as emerin and SUN2 (Fig. 8F). This effect was most likely secondary to nesprin knockdown and probably caused by a loss of nuclear integrity and/or failure of NE reformation after division. Double siRNA increased the severity of the nuclear convolution defects and appeared to cause membrane 'blistering' and 'flaring' (Fig. 8E). These defects were observed with multiple siRNAs to each region (data not shown) and control; scrambled siRNAs had no effect on nuclear morphology (Fig. 8C and D).

Nesprin-1 siRNAs had a dramatic effect on emerin localization and caused similar defects to those observed in EDMD patient fibroblasts with *SYNE* mutations (Fig. 9A–E). siRNA targeted to nesprin-1α caused a significant increase in emerin mislocalization to micronuclei and the cytoplasm when compared with control siRNA. siRNA to nesprin-1β caused emerin to accumulate at a 'honeycombed' polar cap in fibroblasts (Fig. 9C) where it co-localized with SUN2 (Fig. 9D). In U2OS cells, nesprin-1β siRNA caused emerin to mislocalize to multiple micronuclei. This effect observed in >70% of the rapidly dividing U2OS cells but not in controls was potentially caused by the inability of emerin to reform at the NE after division (Fig. 9A). In contrast, nesprin-2 siRNA in both fibroblasts and U2OS diminished emerin levels and caused its loss from patches of the nucleus (Fig. 9B).

TEM shows nuclear membrane defects and changes in the organization of intranuclear heterochromatin

Ultrastructural analysis revealed that both nesprin-1 and -2 siRNAs caused changes in cell and nuclear shape, extensive convolutions of the NE as well as marked changes in the organization and localization of heterochromatin (Fig. 10). Specifically, nesprin-1α siRNAs caused the INM and ONM to become separated, increasing the luminal space from 50 to >300 nm in both fibroblasts and U2OS cells (Fig. 10B and C). Nesprin-1β-targeted siRNA in fibroblasts resulted in loss of NE integrity. Large regions of NE at a pole of the nucleus was unformed resulting in a discontinuous membrane, an observation consistent with the mislocalization of emerin to a honeycombed polar cap. Dramatic changes in heterochromatin organization, including an increase in width and density of the heterochromatin underlying the INM as well as dense patches of intranuclear heterochromatin, were also induced (Fig. 10E and F). Nesprin-2 siRNA caused NE convolutions and discontinuities. The nuclear membranes appeared disorganized, fragmented and vesiculated, and the association of heterochromatin with the membranes was patchy. These same membrane defects were also observed in cytoplasmic organelles, particularly the ER and mitochondria with vesiculation making it difficult in regions close to the nucleus to discriminate between these different membranous compartments (Fig. 10H and I).

DISCUSSION

Nesprin/emerin/lamin interactions

The identification of unique *SYNE1* and *SYNE2* sequence variants in patients with EDMD and EDMD-like phenotypes implicates nesprins in this complex neuromuscular disease and provides new and important insights into the aetiology of laminopathies. To date, two non-mutually exclusive hypotheses have been proposed to account for how mutations in genes encoding ubiquitously expressed NE proteins such as emerin and lamins A/C result in the muscle-specific defects seen in EDMD (26). The first suggests disruption of INM complexes and the nuclear lamina causes disorganization of nuclear heterochromatin and changes in gene expression, whereas the second proposes that the mechanical strength of the cell nucleus is compromised when the nuclear lamina is weakened, leading to structural and adaptive signalling defects in mechanically stressed tissues such as muscle. Using patient fibroblasts and siRNA, we were able to implicate nesprins as mediators of both

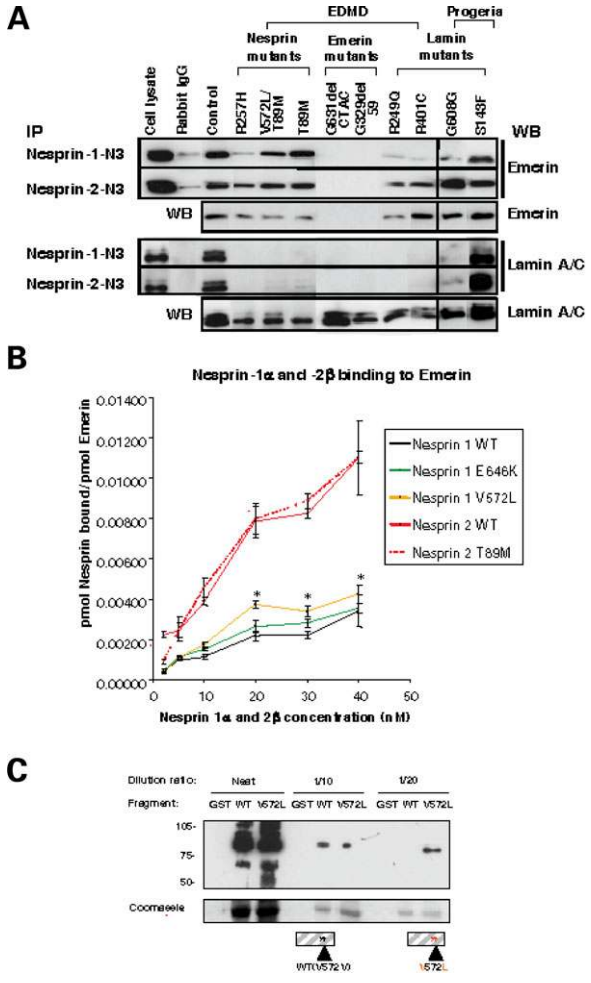

Figure 7. Nesprin/emerin/lamin interactions are changed *in vitro* and *in vivo*. (**A**) Immunoprecipitation using nesprin-1 and -2 antibodies followed by western blotting with emerin and lamin A/C antibodies demonstrates that binding of nesprin-1 to emerin is impaired in some extracts from patients with both *SYNE* and *LMNA* mutations. Nesprin-2 binding is relatively unaffected (top panels). Binding of both nesprin-1 and -2 to lamin A/C in fibroblasts from patients with EDMD caused by either *SYNE*, *EMD* or *LMNA* mutations is impaired. This contrasts with binding in extracts from patients with *LMNA* mutations causing progeria syndromes, where lamin and nesprin binding was relatively unaffected when compared with control (bottom panels). Antibodies for western blotting (WB) are emerin in top panels and lamin A/C in bottom panels as indicated. (**B**) Using a quantitative plate-binding assay, nesprin-2β was shown to bind more strongly to emerin than nesprin-1α. In addition, a nesprin-1α construct harbouring the *SYNE1* V572L mutation bound more strongly than wild-type to emerin. Results are presented as mean ± SEM. $^{*}P < 0.05$ was defined as statistical significance analysed by general linear modelling (*post hoc* tests). Each significant *P*-value (nesprin-1 V572L versus wild type mean binding affinity at a concentration of 23.1 pmol emerin) is as follows for different nesprin-1α concentrations: 20 nM, $P < 0.005$; 30 nM, $P < 0.05$; 40 nM, $P < 0.05$. (**C**) Gel overlay assay demonstrating binding of a recombinant nesprin-1 fragment (amino acids 373–627) that is the minimal nesprin-1/emerin binding region to emerin. A fragment harbouring the *SYNE1* V572L mutation binds more strongly to emerin when compared with wild-type shown by increasing the dilution of recombinant protein.

processes by showing that defective or absent nesprin-1 or -2 caused nuclear morphology defects, mislocalization of both emerin and lamin A/C, reorganization of nuclear heterochromatin and loss of NE integrity, resulting in uncoupling of the nucleoskeleton and cytoskeleton.

A distinctive feature of myoblasts and fibroblasts from EDMD patients with *SYNE* mutations was loss and mislocalization of emerin from the NE. These defects mimic the phenotype of fibroblasts derived from patients with XL-EDMD, where >95% of mutations in *EMD* cause absence or mislocalization of emerin from the NE (3). The importance of nesprin in stabilizing emerin at the NE is supported by nesprin overexpression and siRNA, both causing loss of NE emerin. Previous studies have shown that INM nesprin-1α is the strongest emerin-binding partner with an equilibrium affinity of 4 nM; however, this study suggests that nesprin-2β may bind even more strongly (19). Recent data also show that recombinant emerin proteins expressed *in vitro* with missense or frameshift mutations exhibit altered binding to both nesprin-1 and -2 when compared with wild-type, implicating defects in emerin–nesprin binding in XL-EDMD (25). Additionally, we were able to demonstrate that a valine–leucine substitution in nesprin-1α resulted in increased binding to emerin. As mutations in *EMD* cause EDMD exclusively, these results suggest perturbed emerin–nesprin interactions at the INM because amino acid changes in their respective binding domains may be central in causing muscle cell dysfunction.

However, disrupted emerin–nesprin interactions are clearly not the only defect in EDMD. Like emerin, nesprins also bind to lamin A/C and are dependent on lamin A for retention at the INM (11). siRNA knockdown of nesprins led to similar nuclear defects induced if lamin A/C is knocked down in mice or *in vitro*. Loss of NE nesprin was observed in a significant proportion of EDMD patient fibroblasts harbouring *SYNE*, *LMNA* and *EMD* mutations, and total loss of NE nesprin-1 has also been described in fibroblasts from an embryonic lethal patient homozygous for a nonsense mutation in *LMNA* (22). Defects in nesprin/emerin/lamin interactions were also demonstrated by co-immunoprecipitation in extracts from EDMD patient fibroblasts, further suggesting a weakening of nesprin–lamin interactions. Although these immunoprecipitation (IP) data need to be interpreted with caution due to the insoluble nature of NE lamins, taken together this evidence points to the importance of the nesprin/emerin/lamin complex in maintaining nuclear stability. Moreover, the apparent dominance of *SYNE* mutations suggests a dominant-negative effect, whereby partially compromised nesprins saturate available SUN proteins while failing to bind emerin and/or lamin A/C correctly. Missense mutations could cause a gain- or loss-of-function effect, whereby emerin or lamin binding to nesprin is enhanced or reduced. Both scenarios would be predicted to alter nuclear strength and integrity, leading to adaptive alterations in cytoskeletal structure (27–29). The similarities in the defects observed in patient fibroblasts and after nesprin siRNA support this idea. In addition, subtle changes in isoform production caused by 5′-UTR sequence variants or alternate translation initiation predicted by the *SYNE2* T89M mutation leading to an N-terminally truncated protein could also alter nesprin interactions at the NE. Taken together, these observations suggest that changes in the binding stoichiometry of the nesprin/emerin/lamin complex at the NE is a feature of EDMD. As the emerin and lamin binding sites in nesprin-1 and -2 overlap and the nesprin and lamin binding sites in emerin overlap, there is likely to be competition for binding

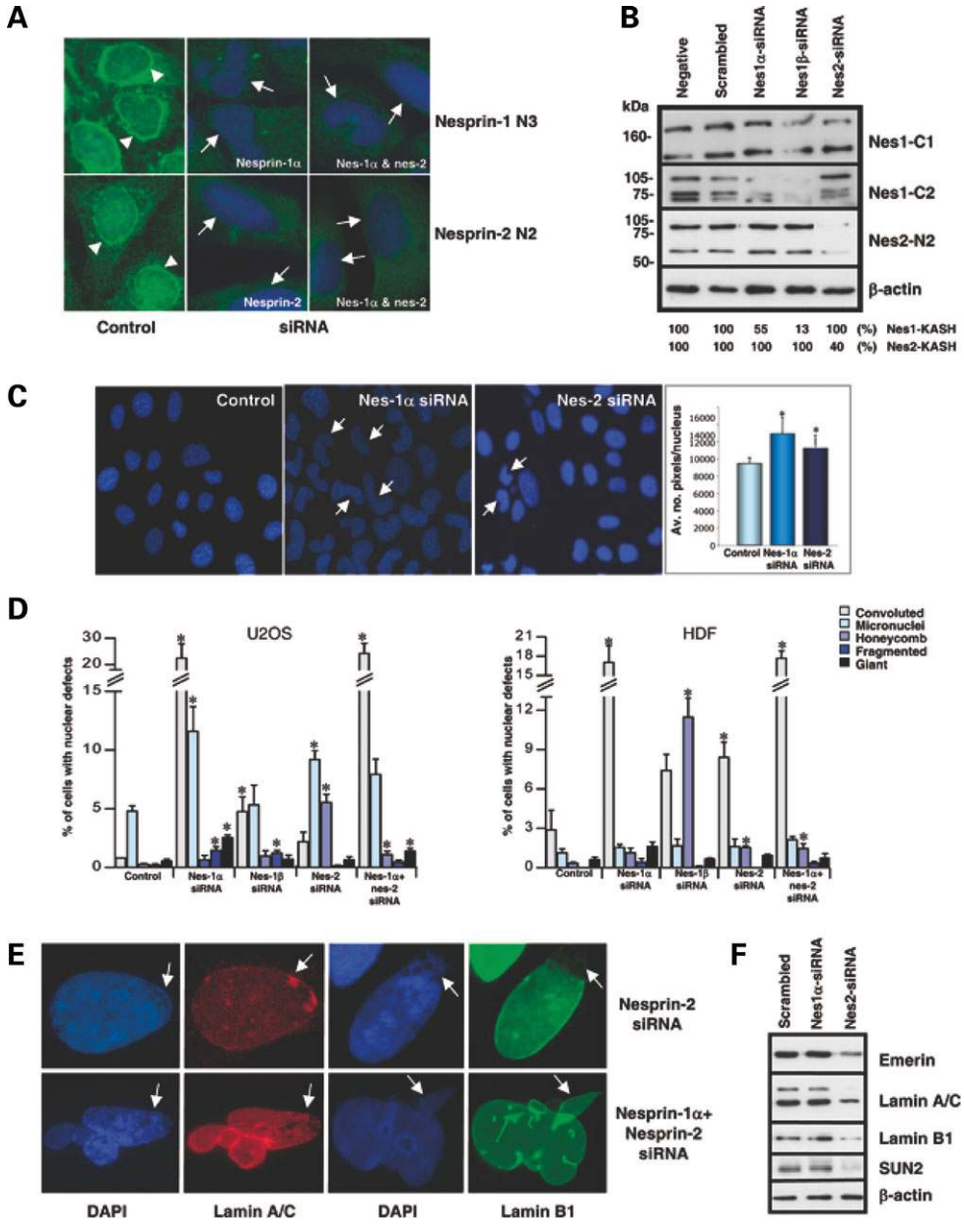

Figure 8. siRNA knockdown of nesprin-1 and -2 in fibroblasts and U2OS cells causes nuclear morphology defects and lamin mislocalization. (**A**) Immunofluorescence at equivalent exposure times showing that in U2OS cells, siRNA to nesprin-1 or -2 reduces NE nesprin-1 and -2 staining, respectively (arrowed), compared with control-treated cells (arrowhead) with cytoplasmic nesprin staining relatively unaffected. (**B**) Western blot in U2OS cells demonstrating specific knockdown of nesprin-1 and -2 isoforms after siRNA treatment. Nesprin-1α siRNA reduces bands of ∼100 and 53 kDa corresponding to nesprin-1α and -1α3SR as well as an additional smaller band. Nesprin-1β siRNA reduces these bands to a greater extent than nesprin-1α-targeted siRNA and, in addition, diminishes bands of ∼146 kDa corresponding to nesprin-1Δβ13SR as well as a larger band >200 kDa. Nesprin-2 siRNA diminished bands of 62 and 87 kDa corresponding to isoforms-2α and -2β. No effect was seen with scrambled control siRNA. RNA levels assessed by qRT–PCR are shown below. (**C**) DAPI staining showing nuclear morphology defects induced by nesprin-1α (large convoluted nuclei and weak DAPI staining, second panel arrowed) and nesprin-2 siRNAs (convoluted nuclei and dense DAPI staining, third panel arrowed) in U2OS cells. Graph shows the significant increase in nuclear size induced by both siRNAs. $^*P < 0.05$ analysed by independent samples *t*-test. $N = 100$ in three independent experiments. (**D**) The frequency of the nuclear morphology defects induced by nesprin siRNAs in both U2OS cells and fibroblasts (HDF). The nuclear defects after each siRNA treatment were quantitated by counting $N = 500$ nuclei in three independent experiments. The results are presented as mean ± SEM. $^*P < 0.05$ was defined as statistical significance analysed by independent samples *t* test. Each significant *P*-value (siRNA versus control) is as follows: for convoluted nuclei: nesprin-1α, $P = 0.016$, nesprin-1β, $P = 0.033$, nesprin-1α + nesprin-2, $P = 0.003$ in U2OS cells; nesprin-1α, $P = 0.009$, nesprin-2, $P = 0.044$; nesprin-1α + nesprin-2, $P = 0.001$ in fibroblasts; for micronuclei: nesprin-1α, $P = 0.034$, nesprin-2, $P = 0.008$ in U2OS cells; for honeycomb: nesprin-2, $P = 0.002$, nesprin-1α+ nesprin-2, $P = 0.048$ in U2OS cells; nesprin-1β, $P = 0.002$; nesprin-2, $P = 0.001$; nesprin-1α + nesprin-2, $P = 0.034$ in fibroblasts; for fragmented: nesprin-1α, $P = 0.015$, nesprin-1β, $P = 0.014$ in U2OS cells; for giant nuclei: nesprin-1α, $P = 0.003$, nesprin-1α + nesprin-2, $P = 0.041$ in U2OS cells. (**E**) Honeycombing of the nucleus and mislocalization of lamins A/C and B (arrowed) induced by nesprin-2 siRNA in U2OS cells are shown in the top panels. Double siRNA for nesprin-1α and nesprin-2 in U2OS cells (bottom panels) increased the gross nuclear convolution defects (lamin A/C staining) and caused nuclear membrane blistering and large nuclear membrane flares (lamin B1 staining arrowed) when compared with single siRNAs. (**F**) siRNAs that induced honeycombing were associated with a reduction in the levels of nesprin NE binding partners including lamins, emerin and SUN2. U2OS cell extracts shown.

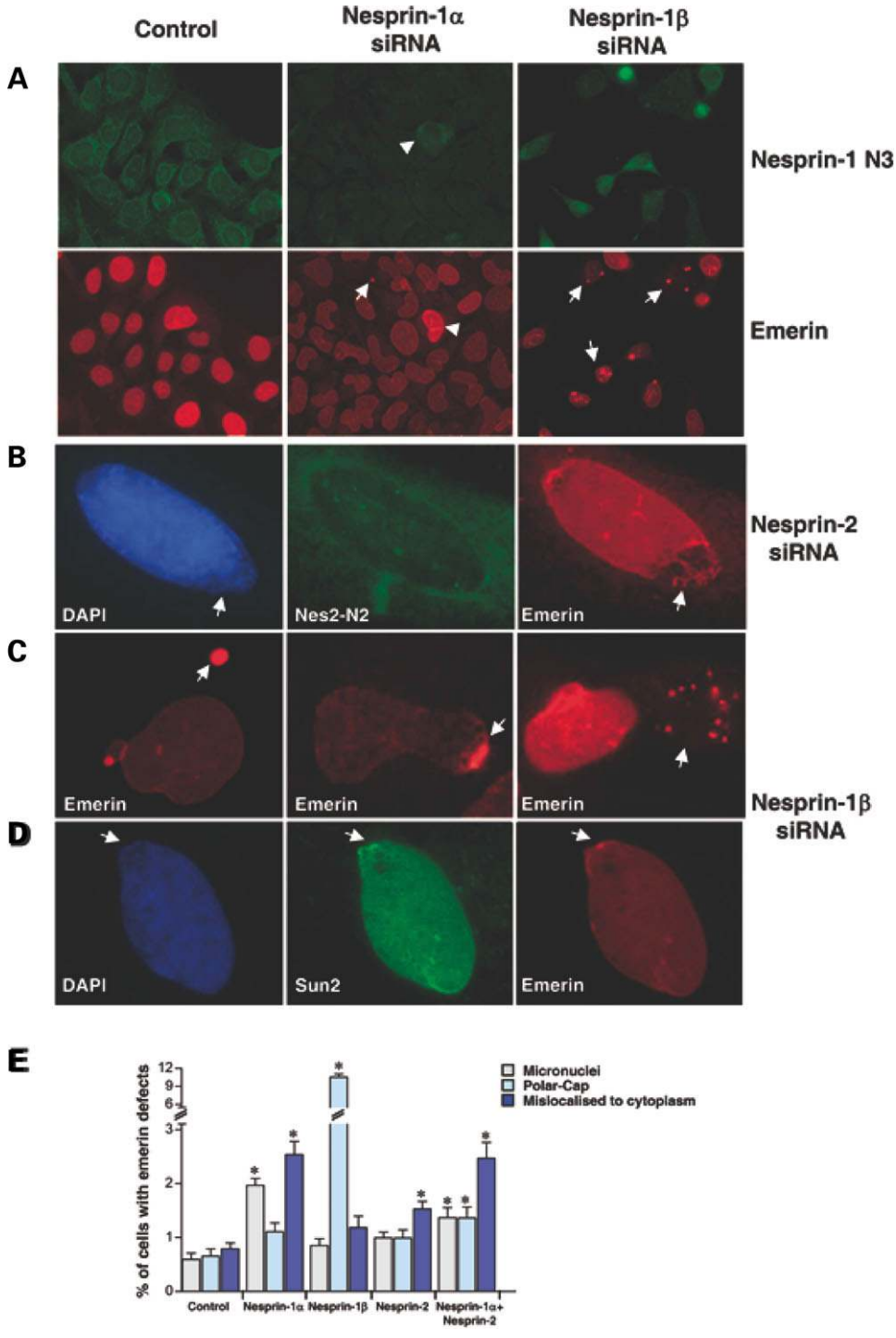

Figure 9. Emerin and SUN2 are mislocalized by nesprin siRNA. (**A**) Emerin defects induced by siRNAs to nesprin-1α and nesprin-1β in U2OS cells. Emerin loss from the NE was observed in >80% of cells after treatment. After nesprin-1α siRNA emerin staining was weak at the NE (normal cell arrowhead in panels) and often mislocalized to micronuclei. After nesprin-1β siRNA emerin was mislocalized to multiple micronuclei (arrowed). (**B**) Emerin defects induced by nesprin-2 siRNA in U2OS cells included loss of NE emerin in large polar patches. (**C**) Emerin defects induced in fibroblasts by nesprin siRNAs reiterated those observed in patient fibroblasts. Defects included micronuclei (first panel arrowed), polar-cap localization (centre panel arrowed) and mislocalization to the cytoplasm (last panel arrowed). (**D**) SUN2 was found to co-localize with emerin in polar caps in a pattern identical to that observed in patient fibroblasts. (**E**) Emerin defects were observed in a significant portion of cells after nesprin-1 siRNAs in fibroblasts. Five hundred cells were counted per treatment in three independent experiments and results are shown as mean ± SEM. $^{*}P < 0.05$ was defined as statistical significance analysed by independent samples *t*-test. Each significant *P*-value (siRNA versus control) is as follows: for micronuclei: nesprin-1α, $P = 0.001$; nesprin-1α + nesprin-2, $P = 0.024$; for polar-cap: nesprin-1β, $P < 0.0001$; nesprin-1α + nesprin-2, $P = 0.042$; for mislocalized to cytoplasm: nesprin-1α, $P = 0.003$, nesprin-2, $P = 0.016$, nesprin-1α + nesprin-2, $P = 0.006$.

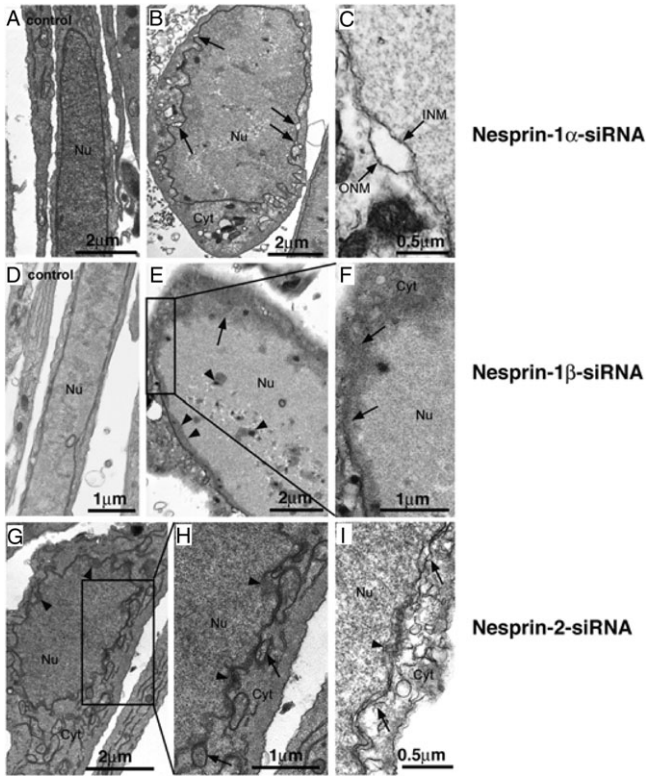

Figure 10. Transmission electron microscopy of siRNA effects in U2OS cells and fibroblasts. (**A**) Control U2OS cell. (**B**) Nesprin-1α siRNA in U2OS cells showing increased cell size, cell and nuclear morphology changes and separation of the INM and ONM. Separation is enlarged in (**C**) (arrowed). (**D**) Control fibroblast. (**E**) Nesprin-1β siRNA in fibroblasts showing loss of NE integrity at one end of the cell (arrowed) and reorganization of nuclear heterochromatin (arrowheads). Loss of NE integrity is enlarged in (**F**). This phenotype was apparent in >60% of cells under EM and was not due to plane of section artefact. (**G**) Nesprin-2 siRNA in U2OS cells showing convolutions of the NE, loss of NE integrity and vesiculation of ONM and ER membranes (arrowed) as well as reorganization of nuclear heterochromatin (arrowhead). Enlargement shown in (**H**). (**I**) Enlargement of another cell showing discontinuities (arrowed) and vesiculation of nuclear membranes and ER.

(19,20,25). This, coupled with the fact that multiple nesprin isoforms may be involved in dynamic interactions with both lamin and emerin at the NE, as well as with each other, makes it likely that even small changes in binding, like those demonstrated in our *in vitro* assays, will affect the overall stoichiometry of the complex (19). The diminution of lamins A/C and B, emerin and SUN2 in the honeycombed nucleus after nesprin siRNA also supports the contention that stable and balanced complexes of nesprin-binding proteins are essential to maintain NE homeostasis. The mislocalization of SUN2 in patient fibroblasts and after nesprin-1 siRNA suggests that SUN2 is also an important component of the nesprin/emerin/lamin complex disrupted in EDMD and that SUN-domain proteins as obvious candidate genes for EDMD.

Nesprins couple the nucleoskeleton to the cytoskeleton

In EDMD, muscle-specific symptoms are not usually apparent at birth and this has led to the hypothesis that impaired nuclear stability and impaired protective and adaptive signalling pathways in these contractile tissues sensitize them to mechanical stresses (28,30). Three independent studies have demonstrated that nesprins in combination with two SUN-domain proteins, SUN1 and SUN2, form a linking complex that couples the nucleoskeleton to the cytoskeleton (31–33). In this study, knockdown of nesprin-1, which was likely to affect both INM and ONM isoforms, resulted in a separation of the INM from the ONM, implying uncoupling of the nucleoskeleton from the cytoskeleton and supporting a central role for nesprins in maintaining these links. This phenotype has also been observed in muscle tissue of $LMNA^{-/-}$ mice and with siRNA knockdown of both SUN1 and SUN2 (31,34).

Importantly, defects in the mechanical coupling between the extracellular matrix and the nucleus mediated through focal adhesion sites and the cytoskeleton leading to defective NFκB signalling have been reported in $LMNA^{-/-}$ and $EMD^{-/-}$ fibroblasts (28,29). Defects in the organization of cytoskeletal components in $LMNA^{-/-}$ fibroblasts have also been shown and it was originally proposed that these defects might be due to disruption of mechanical connections between integrins, cytoskeletal filaments and the nucleus (27,35). Previously, giant scaffold proteins mutated in Duchenne muscular dystrophy, such as dystrophin and spectrin, were suggested as candidates for these connections. However, accumulating evidence strongly implicates multiple nesprin isoforms as mediators of these connections. Knockdown of the *Drosophila* nesprin orthologue MSP300 results in defective muscle/tendon connections and defects in integrin localization at the plasma membrane (36). Indeed, defects in mechano-sensitive signal transduction pathways are a common feature of most muscular dystrophies, and the uncoupling of cytoskeletal signalling via nesprins, predicted from our model of EDMD, provides a common mechanistic pathway for the muscular dystrophies induced by NE defects (21,37). Further studies investigating the effects of nesprin knockdown on signal transduction in muscle cells should help in testing this hypothesis.

siRNA to nesprin-1β and nesprin-2 also resulted in changes in the distribution of NE and intranuclear heterochromatin and lamins, implicating nesprins in the gene-expression mechanistic pathway proposed for EDMD. Heterochromatin changes could have been caused in part by mislocalization of emerin, which connects via its LEM (LAP2-emerin-MAN1) domain and barrier to autointegration factor to heterochromatin (38). Alternatively, the failure of nesprin antibodies to IP lamins may indicate that nesprin binding to the more soluble intranuclear lamins is perturbed in EDMD, supporting the notion that nesprins may act as a scaffold for the nucleoskeleton composed of spectrins, actin and lamins. Disruption of the integrity of this structure would result in chromatin reorganization, changes in gene expression and nuclear disorganization leading to disrupted signalling pathways, cell cycle progression and nuclear export (21,39).

Multiple functions for nesprins in muscle

Although causality for nesprin missense mutations in EDMD cannot be confirmed from this study because of the small number and size of the pedigrees, there is strong evidence implicating them in the disease. The missense mutations found in *SYNE1* and *SYNE2* occurred at positions that are highly conserved evolutionarily and which lie within the

lamin and emerin binding domains of nesprin-1 and -2. Indeed, the three missense mutations in nesprin-1 were clustered within this domain with no mutations found within the remaining domains of the much larger nesprin-1β isoform. Even if these *SYNE* sequence variants represent rare polymorphisms, the variable phenotypic expression and high proportion of EDMD and EDMD-like patients without *EMD* or *LMNA* mutations are in keeping with the hypothesis that multiple genetic modifiers affect the EDMD phenotype. The possibility that nesprins are genetic modifiers is supported by the identification of a double heterozygote proband with mutations in both *SYNE1* and *SYNE2*, who exhibited the most severe disease phenotype and defects in nuclear morphology and emerin localization. Other genetic modifiers known to increase the severity of EDMD include lamin in XL-EDMD and desmin, a muscle sarcomeric protein, in AD-EDMD (40). This is particularly relevant as the unique nature of nesprin isoform production means that the amino acid substitutions identified in nesprins will also affect multiple ONM and sarcomeric isoforms and therefore impinge on other muscle functions. Therefore, the marked heterogeneity in patient phenotype observed in nesprin mutant patients might be predicted as their phenotypic expression is likely to be dependent on the specific isoforms and the interactions most affected. For example, in the muscle sarcomere, nesprins act as scaffolds and bind proteins, such as titin, that are important for structural integrity (15). In the sarcoplasmic reticulum and ONM, a nesprin-1α-like isoform scaffolds a signalling complex containing muscle-specific A-kinase anchoring protein and the ryanodine receptor that is important for muscle cell contraction (41). ONM nesprins act to regulate nuclear migration, an essential process during muscle differentiation, with defective nuclear localization, a feature of EDMD skeletal muscle (42). EDMD is a neuromuscular disorder and nesprin-1 is highly concentrated at the neuromuscular junction (NMJ) (13,43). A recent study implicates *SYNE1* mutations in autosomal-recessive cerebellar ataxia, a neuronal disorder. However, there were also defects in nuclear localization at the NMJ in the single patient studied (44). These mutations occur in more N-terminal regions of the giant protein outside the emerin and lamin binding domains and are likely to result in severe loss of function of the larger isoforms and may also affect brain-specific isoforms. Mice with deletions of both *SYNE1* and *SYNE2* KASH domains also exhibit defects in myonuclear anchorage and distribution and are neonatal lethal because of defects in motor neuron innervation (45). Future studies including further genetic screening of nesprins in EDMD, including pedigrees with previously identified *LMNA* mutations, and in laminopathies including dilated cardiomyopathy (DCM) and related syndromes should lead to further dissection of the complex mechanisms involved in these heterogeneous disorders.

MATERIALS AND METHODS

Patients

Patients for this study were selected on the basis of the results of a routine diagnostic mutational analysis of *EMD* and *LMNA* in the framework of a National (MD-NET) and a European (MYOCLUSTER/EUROMEN) research network dedicated to investigate muscular dystrophies and particularly EDMD. Out of 271 unrelated predominantly Caucasian index cases clinically expressing EDMD or related phenotypes, 36 *EMD* and 31 *LMNA* mutations were identified, resulting in a detection rate of 24.6% for both genes. Thus, the disease was not associated with either *EMD* or *LMNA* in more than 60% of EDMD patients. About 190 of the patients negative for *EMD* and *LMNA* mutations were included in a functional candidate gene approach and tested for 21 candidate genes among them *SYNE1* and *SYNE2*. All materials (blood, skin biopsies and muscle biopsies) of the patients and controls included in this study were taken with informed consent of the donors and with approval of the local ethical board.

All patients used in this study are listed in Supplementary Material, Table S1. The clinical features of patients with *SYNE1* and *SYNE2* mutations were within the diagnostic criteria for EDMD despite the variable clinical expression and are detailed in Supplementary Material.

Mutation analysis

Primer pairs for RT–PCR were designed for all the exons and flanking intronic sequences and UTRs of nesprin-1α_1, 1α_2, 1$\alpha_1\Delta3$, 1β_1, 1β_2, 1$\beta_1\Delta13$, nesprin-2α_1, 2α_2, 2β_1 and 2β_2. One hundred and eighty oligonucleotide primers from intronic sequences for 88 exons were designed using the program Primer3Input (primer3_www.cgi, version 0.2) (Supplementary Material, Table S2). The PCR reaction was carried out in an automated thermal cycler (Perkin Elmer 9600 or 9700). Genomic DNA was amplified by the following thermal profile: denaturation at 95°C for 3 min, then further denaturation for 40 s, annealing at the appropriate temperature (55–59°C) for 40 s and extension at 72°C for 1.5 min followed by a final extension step of 5 min at 72°C for 30 cycles. Aliquots of 25 μl of standard PCR reaction contained 75 mM Tris–HCl (pH 8.8), 20 mM $(NH_4)_2SO_4$, 2.0 mM $MgCl_2$, 0.25 mM dNTP, 6.5 pmol of each forward and reverse primer, 150 ng of genomic DNA as template and 0.75 U of *Taq* DNA polymerase (Fermentas). To check the PCR efficiency, 10 μl of aliquots were analysed by agarose gel electrophoresis.

Heteroduplex analysis

Heteroduplex analysis was modified as follows. The PCR products of a test sample and a wild-type control were mixed (1:1) and heat denatured for 2 min at 95°C. After reannealing for 30 min at 37°C, the reaction was stopped by adding a stop mix (5:1) consisting of 95% formamide, 0.25% Bromophenol blue, 0.25% xylene cyanol and 10 mM NaOH. Then, 10 μl of the reannealed samples was loaded onto a non-denaturing polyacrylamide gel (Serdogel, Serva) and electrophoretically separated at 300–600 V in 0.6× TBE according to the recommendations of the supplier. After electrophoresis, DNA fragments were visualized under UV light by ethidium bromide staining and photographed. Mutations were distinguished from wild-type homoduplexes by shifted extra bands.

Sequence analysis

Double-stranded PCR products that showed abnormal heteroduplex patterns were purified and concentrated for sequencing using 'Microcon 100' columns (AMICON GmbH). PCR products were sequenced by automated fluorescent DNA sequencing technology (Perkin Elmer, Applied Biosystems). The sequence reaction was performed using an ABI PRISM BigDye Terminator Cycle Sequencing Ready Reaction Kit. Oligonucleotides used for PCR were also used as primers for bidirectional sequencing of the individual exons. Reactions were evaluated by an automated 310 DNA Sequencer (Applied Biosystems) according to manufacturer's instructions. To prove the validity of the DNA variations found, the PCR fragments were digested with appropriate restriction endonucleases. Additionally, all variations were tested for their frequency in 384 alleles of a Caucasian (German) reference population. Segregation of the DNA variations was analysed in the patient's families if available.

Cell culture

Subcutaneous fibroblasts from patients with different laminopathies and from control individuals (Supplementary Material, Table S1) were obtained from skin biopsies. The biopsies were minced with a razor blade, explanted into Petri dishes and grown in Dulbecco's modified Eagle's medium (DMEM) supplemented with 50 μg/ml ampicillin, 50 μg/ml streptomycin and 10% fetal calf serum (FCS). Cultures were analysed between passages 8 and 22. For cell phenotype analysis, six independent experiments were scored by counting $N = 500$ cells per experiment. Scoring was performed by at least two independent observers blinded to sample identity. Defects were scored on three occasions between passages 11 and 14 to rule out passaging artefacts. Primary myoblast cell lines were obtained from skeletal muscle biopsies taken for muscle histology of the patients described. By digestion with trypsin/EDTA, cells were extracted from the tissue and washed in DMEM supplemented with 10% FCS and 50 μg/ml gentamycin. The isolated muscle cells were then grown in the skeletal muscle cell growth medium (C-23060, PromoCell) supplemented with 1× L-glutamine, 50 μg/ml gentamycin and 10% FCS. Myotubes were induced for 7 days by using the skeletal muscle cell differentiation medium (C-23061, PromoCell) supplemented with 1× L-glutamine and 50 μg/ml gentamycin. Differentiation was measured by scoring myotubes at 10 random fields in five independent experiments. Myotubes were identified by staining with marker proteins myosin and α-sarcomeric actin.

Antibodies, western blotting and immunoprecipitation

Rabbit antibodies to human nesprin-1 and nesprin-2 were generated against five synthetic polypeptides: nesprin-1: C1, C2, N3 and nesprin-2: N2, N3, as described previously (Immune Systems Ltd, Paignton, UK) (10,11). Each polypeptide was conjugated to keyhole limpet haemocyanin, and the conjugates were injected into rabbits to produce polyclonal antibodies, which were subsequently affinity-purified and enzyme-linked immunosorbent assay tested to confirm specificity. Western blots were performed on cell lysates after siRNA according to standard procedures. Nesprin-1 and -2 were detected using the above nesprin antibodies (diluted 1:800–1:2500), followed by incubation with a horseradish peroxidase-conjugated anti-rabbit IgG secondary antibody diluted 1:2000 (NA934, Amersham Pharmacia Biotech). Other antibodies were lamin A/C (Jol2, Serotec), lamin B-1 (ab16084, abcam) and emerin 4G5 (NCL-Emerin, Novacastra). The loading control antibody was β-actin (Sigma). Antibody specificity controls were performed by pre-incubation with peptides. The ECL or ECL^{+Plus} chemiluminescent kit (Amersham Pharmacia Biotech) was used for signal detection accordingly.

Confluent HDFs were harvested, treated with IP buffer (10 mM HEPES, pH 7.4, 10 mM KCl, 5 mM EDTA, 1% Triton X-100 and protease inhibitor cocktail) and sonicated on ice and then centrifuged at 16 000 *g* for 15 min at 4°C. Lysates was then pre-cleared with protein A agarose beads (Roche). IPs with nesprin-1 N3 and nesprin-2 N3 antibodies and rabbit IgG as control (4 μg antibody/100 μg cell lysates) were performed at 4°C overnight, followed by incubation with protein-A agarose beads at 4°C for 2 h and centrifugation at 4000 *g* for 10 min. After washing with IP buffer four times and sedimentation of the protein complexes, the pellets were subjected to 4–15% gradient SDS–PAGE electrophoresis and western blotting was performed, as described earlier.

Immunocytochemistry and confocal microscopy

HDFs were seeded at a density of $1.0–2.0 \times 10^4$ cells/ml on 13 mM diameter cover slips in a 24-well plate, allowed to settle and incubated under normal culture conditions for 1–2 days. Cells were washed with tissue culture grade phosphate-buffered saline (PBS) twice for 5 min each, then fixed immediately in either 50% methanol/50% acetone at −20°C for 5 min or 4% formaldehyde/PBS (37°C pre-warmed) at room temperature (RT) for 10 min and then further washed in PBS for 5 min twice. Cells were permeablized with 0.5% NP-40 in PBS for 3.5 min at RT and washed in PBS for 5 min three times and then blocked in 3% bovine serum albumin (BSA)/PBS for 30–60 min at RT. The cover slip was inverted and placed on top of 30 μl of primary antibody (nesprin-1 C1, N3 diluted 1:80–100; nesprin-2 N2, N3 diluted 1:100–150 in blocking buffer) on a piece of parafilm and incubated overnight at 4°C. Rabbit IgG (I5006, Sigma) was used as a negative control, and peptide blocking with 5–10× peptides specific for nesprin antibodies above ablated all staining.

Frozen sections of fresh human skeletal muscle biopsies from control and patients were placed onto Superfrost and microscope slides, fixed in acetone/methanol (1:1) for 5 min at −20°C and permeablized with 0.5% NP-40/Tris-buffered saline (TBS) (pH 7.6) for 3.5 min at RT. After blocking with 5% normal goat serum/TBS at RT for 30–60 min, sections were incubated at 4°C overnight with primary antibodies to nesprin (as mentioned earlier) and to different cellular regions: emerin 4G5 and lamin A/C (MMS-107P, Covance), lamin B-1 (abcam), SUN1 (gift of Dr Sue Shackleton, University of Leicester), SUN2 (gift of Dr Didier Hodzig, University of Washington), α-sarcomeric actin (Sigma) and Myosin (Alexis Corporation).

Cells and sections were incubated in the dark for 30 min at RT with goat Anti-Rabbit AlexaFluor™ 488 and goat Anti-Mouse AlexaFluor™ 568 secondary antibodies diluted 1:200 in blocking buffer, respectively (Vector Laboratories, Inc.), and then washed in PBS for 5 min twice. All samples were mounted and settled in Mowial mountant containing DAPI and images were digitally captured using Olympus BX51 fluorescence microscope or a Leica TCS-SP1-MP Laser scanning confocal system. Confocal images were captured using a ×63, 1.2 NA, water immersion lens. Alexa dyes were excited simultaneously using 488 and 568 nm laser lines and their emitted light was captured between 510–550 and 610–650 nm, respectively. DAPI-stained nuclei were sequentially excited using a Tsunami (Spectra Physics) multiphoton laser tuned to 720 nm, using a capture window of 400–480 nm.

Plasmid constructs and site-directed mutagenesis

Human cDNAs for enhanced GFP (EGFP)-nesprin-1α, 1β, 1βΔ13SR and 2β constructs were amplified using a high-fidelity GC-rich PCR kit (Roche) and inserted in-frame into *Bgl* II or *Bsp* EI and *Sal* I sites of the pEGFP-C1 vector (Clontech). The nesprin-1 mutant constructs (V572L, E646K) were generated using QuikChange™ XL site-directed mutagenesis kit (Stratagene).

Cell culture and transfection analysis

HDFs and U2OS cells were cultured at 37°C/5% CO_2 in DMEM plus 10% FCS (Sigma). For transient transfection, cells were plated onto chamber slides at 1.2×10^5 cells/ml and transfected using Superfect™ (Qiagen). Twenty-four hours post-transfection, cells were fixed and stained with Emerin antibody (Novacastra) for immunofluorescence, as described earlier.

Plasmid constructs and site-directed mutagenesis

Nesprin-1 and -2 constructs lacking the transmembrane domain were amplified from human cDNA by RT–PCR by using the following primers: nesprin-1α: GTGAACTCATATGAAAGGAGAACGACTGCTAAAGCC and AGATCTATGGATCCCCGGACCGACCTGGCCCTGG and nesprin-2β GTGAACTCATATGGCCATGGAGCGGCGCATGGAAAT and AGATCTATGGATCCCGCTGTGGCCGTGTGCTGCC. Incorporated into the N-terminal PCR primer was an *Nde*1 site at the first methionine, and the C-terminal PCR primer was a *Bam*H1-stop–*Bgl*II restriction site, which allowed both C- and N- terminal histidine tagging. The amplicons were 'A-tailed' and cloned into pGEM-T Easy (Invitrogen) and the insert was verified by sequencing. Specific mutations (nesprin-1: V572L and E646K and nesprin-2: T89M) were introduced using the QuickChange XL site-directed mutagenesis kit (Stratagene). The nesprin constructs were digested with *Nde*1–*Bam*H1 and cloned into bacterial expression vector pET29b (Novagen) at the *Nde*1–*Bgl*II sites. The nesprin-ΔTM protein was in-frame with the C-terminal poly-His tag. In order to clone the nesprin constructs into the pTnT vector (Promega), the genes were amplified from the pGEM-T Easy Nesprin constructs described above using SP6 primer and the following N-terminal nesprin primers containing a Kpn1 and strong Kozak sequence; nesprin1: GGTACCGCCGCCACCATGGGAGAACGACTTGCTAA and nesprin 2: GGTACCGCCGCCACCATGGCCATGGAGCGG CGCAT. The product was then cloned into the *Kpn*1–*Not*1 sites in pTnT. Emerin-ΔTM (residues 1–220) was cloned into pET-11c vector to express His-tagged emerin (kind gift from Dr Juliet Ellis).

Synthesis of ^{35}S-methionine-labelled nesprin in reticuloctye lysate and the purification of recombinant nesprin and emerin from *Escherichia coli*

^{35}S-methionine-labelled wild-type and mutants of nesprin-1 and -2 were generated from the pTnT-Nesprin plasmids using the T7 coupled reticulocyte system, according to manufacturer's instructions (Promega). Protein desalting spin columns (Pierce) were used to remove unincorporated ^{35}S-methionine. Synthesis of full-length labelled nesprin1-ΔTM (residues 1–922) and nesprin2-ΔTM (residues 1–726) were confirmed by direct autoradiography of labelled protein following SDS–PAGE. Western blot was used to determine the concentration of ^{35}S-labelled nesprin using antibodies nesprin-1 N3 and nesprin-2 N2, respectively. For quantitation, the amount of nesprin in the lysate was compared with standard amounts of pure recombinant His-tagged nesprin isolated from *E. coli*. Bands were digitized and the concentration of nesprin in the lysate was calculated. His-tagged nesprin-1ΔTM (residues 1–922) and nesprin-2ΔTM (residues 1–726) were produced in the Rosetta (DE3) tRNA-adapted *E. coli* strain (Novagen) following 24 h: isopropyl-beta-D-thiogalactopyranoside (IPTG) induction at 30°C. The nesprin was eluted from a 1 ml HisTrap HP column (Amersham) and fractions were analysed for purity by SDS–PAGE. Purified nesprin was dialysed against 150 mM NaCl, 10 mM dithiothreitol, 20 mM Tris, pH 7.5, to remove imidazol and then snap frozen in LqN_2 and stored at −80°C. Emerin-ΔTM (1–220) was expressed in Rosetta (DE3) and purified as described earlier (25).

Plate assay

The protein interaction assay has been described previously (19). Three quantities of recombinant emerin (3.8, 11.5 and 23.1 pmol) diluted in PBS to a 100 μl final volume were bound to Immulon4HBX Flat Bottom 96-well plates overnight at 4°C. The target protein was removed and plates blocked with 300 μl BSA (30 mg/ml) for 6 h. Negative control wells were incubated overnight with BSA alone. The blocking solution was replaced with 'desalted' radioactive nesprin reticulocyte lysates diluted to a final volume of 100 μl in PBS. Six concentrations of nesprin from 2 to 40 nM were investigated in the binding assay, the range being added to each of the three emerin concentrations. The plates were incubated for 2 h at RT and then washed five times with 200 μl binding buffer (20 mM HEPES, pH 7.4, 110 mM potassium phosphate, 2 mM magnesium acetate and 0.5 mM EGTA) to remove unbound protein. Bound proteins were eluted from the wells in 100 μl 5% SDS and radioactivity was measured by scintillation counting. The wells were not allowed to dry out throughout the experiment. The concentrations of

wild-type and mutant nesprin-1ΔTM and nesprin-2ΔTM were shown to be the same by western blotting. Similar efficiencies of synthesis in the reticulocyte lysate were also necessary between constructs, and low expression samples were excluded. Labelled luciferase protein expressed from the pTnT control plasmid was used as a negative control for emerin binding.

Overlay assay

Lysates from BL21 (DE3) cells expressing glutathione *S*-transferase-nesprin fragment 1α residues 373–627 WT or carrying mutation V572L were extracted in SDS–PAGE sample buffer and resolved by 12% SDS–PAGE. Equal amounts of each nesprin fusion protein lysate were loaded on the gel as 'neat', 1:10 or 1:20 dilution. Following transfer to nitrocellulose membrane and blocking with 6% marvel milk in PBS-Tween-20 (0.1%) (PBST), blotted proteins were washed for 2× 5 min with overlay buffer (10 mM Tris, 150 mM NaCl, 1 mM EDTA, 0.1% Tween-20, pH 7.4) and further incubated with His-tagged emerin 1–221 fusion protein diluted in overlay buffer containing 0.2% gelatin overnight at 4°C or for 2 h at RT. The emerin fusion protein was used at a concentration of 5 μg. Membranes were washed with overlay buffer and binding visualized by immunoblotting with anti-emerin antibody AP8.

RNA interference

For the siRNA experiments, oligo's specific for nesprin-1α: 5′-CTGCATAGTACCGAAACCCAA-3′, 5′-CAGGAGCTTC AGAGAGACATA-3′, 5′-CGAGGCAAGTGTAGTCTC-3′ and nesprin-1β: 5′-CAGCCCGTAGCAGAACAAATA-3′, 5′-GA ACTCGCTGAAATCCAA-3′ and nesprin-2α: 5′-CAGAAC TAGTTGATTAGTTTA-3′, 5′-CCCGAGCATCACTACAAG CAA-3′ were purchased from Qiagen or Proligo LLC. For control samples, a non-silencing oligo was used (Qiagen). Oligos were annealed and transfected into control HDFs and U2OS cells using HiPerFect transfection reagent, according to manufacturer's instructions (Qiagen). Seventy-two hours post-transfection, samples were processed for immunofluorescence, western blot and electron microscopy (EM) analysis, as described earlier. Each experiment was performed more than three times. Phenotypes were scored by counting $N = 500$ cells in more than three individual experiments by at least two independent observers blinded to sample identity. Nuclear size was measured by analysis of pixel area using Photoshop software.

Isolation of cytoplasmic RNA

The culture medium was removed from the monolayer of U2OS cells or HDFs before and after siRNA and 1 ml of RNA STAT-60 was pipetted repeatedly over the cells to lyse them. About 200 μl of chloroform was added to the homogenate and the sample vortexed for 15 s to mix before incubating at RT for 5–10 min. The sample was centrifuged at 12 000 *g* for 15 min at 4°C, the aqueous phase removed and incubated at RT for 5–10 min with 500 μl of isopropanol. The sample was centrifuged again at 12 000 *g* for 10 min at 4°C, the supernatant discarded and the pellet washed with 75% EtOH (made with DEPC-treated dH_2O) by vortexing and centrifuging at 7500 *g* for 5 min at 4°C. The pellet was air-dried for 5–10 min, resuspended in 100 μl DEPC-treated dH_2O, the RNA concentration was measured using NanoDrop® Spectrophotometer ND-1000 (Labtech international) and stored at −80°C.

Reverse transcription synthesis of cDNA and real-time quantitative RT–PCR

About 5 μg of each RNA was made up to a volume of 12 μl in DEPC-treated dH_2O, incubated at 65°C for 5 min with 1 μl RNasin and then placed directly in ice. About 0.5 μl random hexamers (0.5 μg/μl), 0.5 μl oligo dT (0.5 μg/μl), 0.5 μl RNasin (40 U/μl), 2 μl dNTPs (10 mM), 4 μl Super RT buffer and 1 μl Super RT enzyme (Promega) were added and the sample incubated at 42°C for 1 h and then 65°C for 5 min. The volume was made up to 100 μl with dH_2O and stored at −20°C. Control reactions without reverse transcriptase/RNA were performed. qPCR amplification for the standard curve and samples were set up in a volume of 20 μl, with 4 μl of cDNA (1:20 dilution), 0.4 μl forward and reverse primer each (10 μM), 10 μl SYBR® GreenER™ qPCR SuperMix Universal (P/N56450, Invitrogen) and 5.2 μl dH_2O performed on Rotor-Gene RG 3000 (Corbett Research) with cycling parameters: 94°C for 15 s, 55°C for 30 s and extension at 72°C for 1 min as well as 86°C for 10 s acquiring to Cycling A(FAM/Sybr) for 45 cycles. 18S was also amplified as normalized control using 18S probe (Taqman) and AmpliTag Gold™ (Roche) under standard reaction conditions.

RT–PCR for tissue expression of nesprin-1 and -2 isoforms

Touchdown PCR was performed on 2 ml of human tisssue cDNA supplied at a concentration of ∼0.1 ng/ml (Clontech) or ∼6.0 ng/μl (Origene) using the GC-rich PCR System (Roche).

Each PCR amplification was set up in a volume of 50 μl with 1 μl 50× dNTPs, 1 μl forward and reverse primer each (10 μM), 5 μl GC-rich buffer, 10 μl 5× PCR buffer, 1 μl enzyme mix and 26 μl dH_2O, then cycled according to the following parameters: 95°C for 3 min, 95°C for 30 s, lowest T_m (melting temperature) of the primer pair—0.2°C/cycle for 1 min, if the product is >3 kb, −68°C for 1 min/kb or if the product is ≤3 kb, −72°C for 1 min/kb. Return to step 2 and cycle 9× and then 95°C for 30 s, lowest T_m −2°C for 1 min, 68 or 72°C for 1 min/kb + 5 s/cycle. Return to step 5 and cycle 24× and then 72°C for 7 min and hold at 4°C.

Electron microscopy

Cells were fixed by immersion in 2% glutaraldehyde containing 2 mmol/l $CaCl_2$ in 0.1 M PIPES buffer at pH 7.4. About 100 μl 33% H_2O_2 was added to each 10 ml aliquot immediately before use. They were fixed *in situ* in culture plates for 2 h at 4°C, rinsed twice in buffer (0.1 M PIPES), scraped free of the plates and transferred to 1.5 ml centrifuge tubes. After buffer washes, cells were post-fixed in 1% osmium

ferricyanide for 1 h, rinsed three times in double distilled water (DIW) and bulk-stained in 2% uranyl acetate for 1 h. They were rinsed in DIW and dehydrated in an ascending series of ethanol solutions to 100% ethanol, rinsed twice in acetonitrile and embedded in quetol epoxy resin. Fifty nanometre sections were cut on a Leica Ultracut UCT, stained with saturated uranyl acetate in 50% ethanol and lead citrate and viewed in an FEI Philips CM100 operated at 80 kV.

Statistics

The percentage of cells with different forms of nuclear and emerin defects between control and each nesprin mutant or siRNA-treated group was analysed by independent samples *t*-test. The differences of mean bound affinity between nesprin and emerin in the plate assays were analysed by general linear modelling (*post hoc* testing) using SPSS 12.0.1 for windows statistical packages. The results were presented as mean $\pm$ SEM. *P* values less than 0.05 were considered statistically significant.

SUPPLEMENTARY MATERIAL

Supplementary Material is available at HMG Online.

ACKNOWLEDGEMENTS

We thank the Muscle Tissue Culture Collection, supported by grants from the 'Deutsche Gesellschaft für Muskelkranke' (Germany) and the 'Association Francaise contre les Myopathies' at the Friedrich-Baur-Institute (Department of Neurology, Ludwig-Maximilians-University, Munich, Germany) for providing the myoblast cell lines. We also thank Dr Kevin O'Shaughnessy for statistical advice.

Conflict of Interest statement. None of the authors of this manuscript has any conflicts of interest to declare.

FUNDING

British Heart Foundation (RG/05/001 and RG/40384 to C.M.S., a BHF Senior Fellow); EC Fifth Framework (QLRT-1999-00870 to C.W. and M.W.); German Network of Muscular Dystrophies funded by the German Ministry of Education and Research (BMBF) (MD-NET, 01GM0302 to C.B. and A.F.). Funding to pay Open Access publication charges for this article was provided by the British Heart Foundation.

REFERENCES

1. McKusick, V.A. (1996) *Mendelian Inheritance in Man*, 11th edn. The John Hopkins University Press, Baltimore and London.
2. Emery, A.E. (2000) Emery–Dreifuss muscular dystrophy—a 40 year retrospective. *Neuromuscul. Disord.*, **10**, 228–232.
3. Bione, S., Maestrini, E., Rivella, S., Mancini, M., Regis, S., Romeo, G. and Toniolo, D. (1994) Identification of a novel X-linked gene responsible for Emery–Dreifuss muscular dystrophy. *Nat. Genet.*, **8**, 323–327.
4. Bonne, G., Di Barletta, M.R., Varnous, S., Becane, H.M., Hammouda, E.H., Merlini, L., Muntoni, F., Greenberg, C.R., Gary, F., Urtizberea, J.A. *et al.* (1999) Mutations in the gene encoding lamin A/C cause autosomal dominant Emery–Dreifuss muscular dystrophy. *Nat. Genet.*, **21**, 285–288.
5. Bonne, G., Mercuri, E., Muchir, A., Urtizberea, A., Becane, H.M., Recan, D., Merlini, L., Wehnert, M., Boor, R., Reuner, U. *et al.* (2000) Clinical and molecular genetic spectrum of autosomal dominant Emery–Dreifuss muscular dystrophy due to mutations of the lamin A/C gene. *Ann. Neurol.*, **48**, 170–180.
6. Capell, B.C. and Collins, F.S. (2006) Human laminopathies: nuclei gone genetically awry. *Nat. Rev. Genet.*, **7**, 940–952.
7. Vytopil, M., Benedetti, S., Ricci, E., Galluzzi, G., Dello Russo, A., Merlini, L., Boriani, G., Gallina, M., Morandi, L., Politano, L. *et al.* (2003) Mutation analysis of the lamin A/C gene (LMNA) among patients with different cardiomuscular phenotypes. *J. Med. Genet.*, **40**, e132.
8. Bonne, G. (2003) The laminopathy saga. *Rev. Neurol.*, **37**, 772–774.
9. Bonne, G., Yaou, R.B., Beroud, C., Boriani, G., Brown, S., de Visser, M., Duboc, D., Ellis, J., Hausmanowa-Petrusewicz, I., Lattanzi, G. *et al.* (2003) 108th ENMC International Workshop, 3rd Workshop of the MYO-CLUSTER project: EUROMEN, 7th International Emery–Dreifuss Muscular Dystrophy (EDMD) Workshop, 13–15 September 2002, Naarden, The Netherlands. *Neuromuscul. Disord.*, **13**, 508–515.
10. Zhang, Q., Skepper, J.N., Yang, F., Davies, J.D., Hegyi, L., Roberts, R.G., Weissberg, P.L., Ellis, J.A. and Shanahan, C.M. (2001) Nesprins: a novel family of spectrin-repeat-containing proteins that localize to the nuclear membrane in multiple tissues. *J. Cell Sci.*, **114**, 4485–4498.
11. Zhang, Q., Ragnauth, C.D., Skepper, J.N., Worth, N.F., Warren, D.T., Roberts, R.G., Weissberg, P.L., Ellis, J.A. and Shanahan, C.M. (2005) Nesprin-2 is a multi-isomeric protein that binds lamin and emerin at the nuclear envelope and forms a subcellular network in skeletal muscle. *J. Cell Sci.*, **118**, 673–687.
12. Zhang, Q., Ragnauth, C., Greener, M.J., Shanahan, C.M. and Roberts, R.G. (2002) The nesprins are giant actin-binding proteins, orthologous to *Drosophila melanogaster* muscle protein MSP-300. *Genomics*, **80**, 473–481.
13. Apel, E.D., Lewis, R.M., Grady, R.M. and Sanes, J.R. (2000) Syne-1, a dystrophin- and Klarsicht-related protein associated with synaptic nuclei at the neuromuscular junction. *J. Biol. Chem.*, **275**, 31986–31995.
14. Wilhelmsen, K., Litjens, S.H., Kuikman, I., Tshimbalanga, N., Janssen, H., van den Bout, I., Raymond, K. and Sonnenberg, A. (2005) Nesprin-3, a novel outer nuclear membrane protein, associates with the cytoskeletal linker protein plectin. *J. Cell Biol.*, **171**, 799–810.
15. Warren, D.T., Zhang, Q., Weissberg, P.L. and Shanahan, C.M. (2005) Nesprins: intracellular scaffolds that maintain cell architecture and coordinate cell function? *Expert Rev. Mol. Med.*, **7**, 1–15.
16. Zhen, Y.Y., Libotte, T., Munck, M., Noegel, A.A. and Korenbaum, E. (2002) NUANCE, a giant protein connecting the nucleus and actin cytoskeleton. *J. Cell Sci.*, **115**, 3207–3222.
17. Padmakumar, V.C., Abraham, S., Braune, S., Noegel, A.A., Tunggal, B., Karakesisoglou, I. and Korenbaum, E. (2004) Enaptin, a giant actin-binding protein, is an element of the nuclear membrane and the actin cytoskeleton. *Exp. Cell Res.*, **295**, 330–339.
18. Mislow, J.M., Kim, M.S., Davis, D.B. and McNally, E.M. (2002) Myne-1, a spectrin repeat transmembrane protein of the myocyte inner nuclear membrane, interacts with lamin A/C. *J. Cell Sci.*, **115**, 61–70.
19. Mislow, J.M., Holaska, J.M., Kim, M.S., Lee, K.K., Segura-Totten, M., Wilson, K.L. and McNally, E.M. (2002) Nesprin-1alpha self-associates and binds directly to emerin and lamin A *in vitro*. *FEBS Lett.*, **525**, 135–140.
20. Libotte, T., Zaim, H., Abraham, S., Padmakumar, V.C., Schneider, M., Lu, W., Munck, M., Hutchison, C., Wehnert, M., Fahrenkrog, B. *et al.* (2005) Lamin A/C-dependent localization of Nesprin-2, a giant scaffolder at the nuclear envelope. *Mol. Biol. Cell*, **16**, 3411–3424.
21. Tzur, Y.B., Wilson, K.L. and Gruenbaum, Y. (2006) SUN-domain proteins: 'Velcro' that links the nucleoskeleton to the cytoskeleton. *Nat. Rev. Mol. Cell. Biol.*, **7**, 782–788.
22. Muchir, A., van Engelen, B.G., Lammens, M., Mislow, J.M., McNally, E., Schwartz, K. and Bonne, G. (2003) Nuclear envelope alterations in fibroblasts from LGMD1B patients carrying nonsense Y259X heterozygous or homozygous mutation in lamin A/C gene. *Exp. Cell Res.*, **291**, 352–362.
23. Ognibene, A., Sabatelli, P., Petrini, S., Squarzoni, S., Riccio, M., Santi, S., Villanova, M., Palmeri, S., Merlini, L. and Maraldi, N.M. (1999) Nuclear changes in a case of X-linked Emery–Dreifuss muscular dystrophy. *Muscle Nerve*, **22**, 864–869.

24. Dabauvalle, M.C., Muller, E., Ewald, A., Kress, W., Krohne, G. and Muller, C.R. (1999) Distribution of emerin during the cell cycle. *Eur. J. Cell Biol.*, **78**, 749–756.
25. Wheeler, M.A., Davies, J.D., Zhang, Q., Emerson, L.J., Hunt, J., Shanahan, C.M. and Ellis, J.A. (2007) Distinct functional domains in nesprin-1alpha and nesprin-2beta bind directly to emerin and both interactions are disrupted in X-linked Emery—Dreifuss muscular dystrophy. *Exp. Cell Res*, **313**, 2845–2857.
26. Gruenbaum, Y., Margalit, A., Goldman, R.D., Shumaker, D.K. and Wilson, K.L. (2005) The nuclear lamina comes of age. *Nat. Rev. Mol. Cell. Biol.*, **6**, 21–31.
27. Broers, J.L., Peeters, E.A., Kuijpers, H.J., Endert, J., Bouten, C.V., Oomens, C.W., Baaijens, F.P. and Ramaekers, F.C. (2004) Decreased mechanical stiffness in LMNA−/− cells is caused by defective nucleo-cytoskeletal integrity: implications for the development of laminopathies. *Hum. Mol. Genet.*, **13**, 2567–2580.
28. Lammerding, J., Schulze, P.C., Takahashi, T., Kozlov, S., Sullivan, T., Kamm, R.D., Stewart, C.L. and Lee, R.T. (2004) Lamin A/C deficiency causes defective nuclear mechanics and mechanotransduction. *J. Clin. Invest.*, **113**, 370–378.
29. Lammerding, J., Hsiao, J., Schulze, P.C., Kozlov, S., Stewart, C.L. and Lee, R.T. (2005) Abnormal nuclear shape and impaired mechanotransduction in emerin-deficient cells. *J. Cell Biol.*, **170**, 781–791.
30. Broers, J.L., Kuijpers, H.J., Ostlund, C., Worman, H.J., Endert, J. and Ramaekers, F.C. (2005) Both lamin A and lamin C mutations cause lamina instability as well as loss of internal nuclear lamin organization. *Exp. Cell Res.*, **304**, 582–592.
31. Crisp, M., Liu, Q., Roux, K., Rattner, J.B., Shanahan, C., Burke, B., Stahl, P.D. and Hodzic, D. (2006) Coupling of the nucleus and cytoplasm: role of the LINC complex. *J. Cell Biol.*, **172**, 41–53.
32. Padmakumar, V.C., Libotte, T., Lu, W., Zaim, H., Abraham, S., Noegel, A.A., Gotzmann, J., Foisner, R. and Karakesisoglou, I. (2005) The inner nuclear membrane protein Sun1 mediates the anchorage of Nesprin-2 to the nuclear envelope. *J. Cell Sci.*, **118**, 3419–3430.
33. Haque, F., Lloyd, D.J., Smallwood, D.T., Dent, C.L., Shanahan, C.M., Fry, A.M., Trembath, R.C. and Shackleton, S. (2006) SUN1 interacts with nuclear lamin A and cytoplasmic nesprins to provide a physical connection between the nuclear lamina and the cytoskeleton. *Mol. Cell. Biol.*, **26**, 3738–3751.
34. Sullivan, T., Escalante-Alcalde, D., Bhatt, H., Anver, M., Bhat, N., Nagashima, K., Stewart, C.L. and Burke, B. (1999) Loss of A-type lamin expression compromises nuclear envelope integrity leading to muscular dystrophy. *J. Cell Biol.*, **147**, 913–920.
35. Maniotis, A.J., Chen, C.S. and Ingber, D.E. (1997) Demonstration of mechanical connections between integrins, cytoskeletal filaments, and nucleoplasm that stabilize nuclear structure. *Proc. Natl Acad. Sci. USA*, **94**, 849–854.
36. Volk, T. (1992) A new member of the spectrin superfamily may participate in the formation of embryonic muscle attachments in *Drosophila*. *Development*, **116**, 721–730.
37. Davies, K.E. and Nowak, K.J. (2006) Molecular mechanisms of muscular dystrophies: old and new players. *Nat. Rev. Mol. Cell. Biol.*, **7**, 762–773.
38. Lee, K.K., Haraguchi, T., Lee, R.S., Koujin, T., Hiraoka, Y. and Wilson, K.L. (2001) Distinct functional domains in emerin bind lamin A and DNA-bridging protein BAF. *J. Cell Sci.*, **114**, 4567–4573.
39. Markiewicz, E., Tilgner, K., Barker, N., van de Wetering, M., Clevers, H., Dorobek, M., Hausmanowa-Petrusewicz, I., Ramaekers, F.C., Broers, J.L. and Blankesteijn, W.M. *et al.* (2006) The inner nuclear membrane protein emerin regulates beta-catenin activity by restricting its accumulation in the nucleus. *EMBO J.*, **25**, 3275–3285.
40. Muntoni, F., Bonne, G., Goldfarb, L.G., Mercuri, E., Piercy, R.J., Burke, M., Yaou, R.B., Richard, P., Recan, D., Shatunov, A. *et al.* (2006) Disease severity in dominant Emery–Dreifuss is increased by mutations in both emerin and desmin proteins. *Brain*, **129**, 1260–1268.
41. Pare, G.C., Easlick, J.L., Mislow, J.M., McNally, E.M. and Kapiloff, M.S. (2005) Nesprin-1alpha contributes to the targeting of mAKAP to the cardiac myocyte nuclear envelope. *Exp. Cell Res.*, **303**, 388–399.
42. Starr, D.A. and Han, M. (2003) ANChors away: an actin based mechanism of nuclear positioning. *J. Cell Sci.*, **116**, 211–216.
43. Grady, R.M., Starr, D.A., Ackerman, G.L., Sanes, J.R. and Han, M. (2005) Syne proteins anchor muscle nuclei at the neuromuscular junction. *Proc. Natl Acad. Sci. USA*, **102**, 4359–4364.
44. Gros-Louis, F., Dupre, N., Dion, P., Fox, M.A., Laurent, S., Verreault, S., Sanes, J.R., Bouchard, J.P. and Rouleau, G.A. (2007) Mutations in SYNE1 lead to a newly discovered form of autosomal recessive cerebellar ataxia. *Nat. Genet.*, **39**, 80–85.
45. Zhang, X., Xu, R., Zhu, B., Yang, X., Ding, X., Duan, S., Xu, T., Zhuang, Y. and Han, M. (2007) Syne-1 and Syne-2 play crucial roles in myonuclear anchorage and motor neuron innervation. *Development*, **134**, 901–908.